Chapter 1

Introduction to OFDM and MIMO-OFDM

1.1 OFDM History

In recent years Orthogonal Frequency-Division Multiplexing (OFDM) [1–4] has emerged as a successful air-interface technique. In the context of wired environments, OFDM techniques are also known as Discrete Multi-Tone (DMT) [5] transmissions and are employed in the American National Standards Institute's (ANSI's) Asymmetric Digital Subscriber Line (ADSL) [6], High-bit-rate Digital Subscriber Line (HDSL) [7], and Very-high-speed Digital Subscriber Line (VDSL) [8] standards as well as in the European Telecommunication Standard Institute's (ETSI's) [9] VDSL applications. In wireless scenarios, OFDM has been advocated by many European standards, such as Digital Audio Broadcasting (DAB) [10], Digital Video Broadcasting for Terrestrial television (DVB-T) [11], Digital Video Broadcasting for Handheld terminals (DVB-H) [12], Wireless Local Area Networks (WLANs) [13] and Broadband Radio Access Networks (BRANs) [14]. Furthermore, OFDM has been ratified as a standard or has been considered as a candidate standard by a number of standardization groups of the Institute of Electrical and Electronics Engineers (IEEE), such as the IEEE 802.11 [15] and the IEEE 802.16 [16] standard families.

The concept of parallel transmission of data over dispersive channels was first mentioned as early as 1957 in the pioneering contribution of Doelz *et al.* [17], while the first OFDM schemes date back to the 1960s, which were proposed by Chang [18] and Saltzberg [19]. In the classic parallel data transmission systems [18, 19], the Frequency-Domain (FD) bandwidth is divided into a number of non-overlapping subchannels, each of which hosts a specific carrier widely referred to as a subcarrier. While each subcarrier is separately modulated by a data symbol, the overall modulation operation across all the subchannels results in a frequency-multiplexed signal. All of the sinc-shaped subchannel spectra exhibit zero crossings at all of the remaining subcarrier frequencies and the individual subchannel spectra are orthogonal to each other. This ensures that the subcarrier signals do not interfere with each other, when communicating over perfectly distortionless channels, as a consequence of their orthogonality [3].

The early OFDM schemes [18–21] required banks of sinusoidal subcarrier generators and demodulators, which imposed a high implementation complexity. This drawback limited the application of OFDM to military systems until 1971, when Weinstein and Ebert [22] suggested that the Discrete Fourier Transform (DFT) can be used for the OFDM modulation and demodulation processes, which significantly reduces the implementation complexity of OFDM. Since then, more practical OFDM

MIMO-OFDM for LTE, Wi-Fi and WiMAX Lajos Hanzo, Yosef Akhtman, Li Wang and Ming Jiang

research has been carried out. For example, in the early 1980s Peled and Ruiz [23] proposed a simplified FD data transmission method using a cyclic prefix-aided technique and exploited reduced-complexity algorithms for achieving a significantly lower computational complexity than that of classic single-carrier time-domain Quadrature Amplitude Modulation (QAM) [24] modems. Around the same era, Keasler *et al.* [25] invented a high-speed OFDM modem for employment in switched networks, such as the telephone network. Hirosaki designed a subchannel-based equalizer for an orthogonally multiplexed QAM system in 1980 [26] and later introduced the DFT-based implementation of OFDM systems [27], on the basis of which a so-called groupband data modem was developed [28]. Cimini [29] and Kalet [30] investigated the performance of OFDM modems in mobile communication channels. Furthermore, Alard and Lassalle [31] applied OFDM in digital broadcasting systems, which was the pioneering work of the European DAB standard [10] established in the mid-1990s. More recent advances in OFDM transmission were summarized in the state-of-the-art collection of works edited by Fazel and Fettweis [32]. Other important recent OFDM references include the books by Hanzo *et al.* [3] and Van Nee *et al.* [4] as well as a number of overview papers [33–35].

OFDM has some key advantages over other widely used wireless access techniques, such as Time-Division Multiple Access (TDMA) [36], Frequency-Division Multiple Access (FDMA) [36] and Code-Division Multiple Access (CDMA) [37, 38, 40–42]. The main merit of OFDM is the fact that the radio channel is divided into many narrowband, low-rate, frequency-non-selective subchannels or subcarriers, so that multiple symbols can be transmitted in parallel, while maintaining a high spectral efficiency. Each subcarrier may deliver information for a different user, resulting in a simple multiple-access scheme known as Orthogonal Frequency-Division Multiple Access (OFDMA) [43–46]. This enables different media such as video, graphics, speech, text or other data to be transmitted within the same radio link, depending on the specific types of services and their Quality-of-Service (QoS) requirements. Furthermore, in OFDM systems different modulation schemes can be employed for different subcarriers or even for different users. For example, the users close to the Base Station (BS) may have a relatively good channel quality, thus they can use high-order modulation schemes to increase their data rates. By contrast, for those users that are far from the BS or are serviced in highly loaded urban areas, where the subcarriers' quality is expected to be poor, low-order modulation schemes can be invoked [47].

Besides its implementational flexibility, the low complexity required in transmission and reception as well as the attainable high performance render OFDM a highly attractive candidate for high-data-rate communications over time-varying frequency-selective radio channels. For example, in classic single-carrier systems, complex equalizers have to be employed at the receiver for the sake of mitigating the Inter-Symbol Interference (ISI) introduced by multi-path propagation. By contrast, when using a cyclic prefix [23], OFDM exhibits a high resilience against the ISI. Incorporating channel coding techniques into OFDM systems, which results in Coded OFDM (COFDM) [48, 49], allows us to maintain robustness against frequency-selective fading channels, where busty errors are encountered at specific subcarriers in the FD.

However, besides its significant advantages, OFDM also has a few disadvantages. One problem is the associated increased Peak-to-Average Power Ratio (PAPR) in comparison with single-carrier systems [3], requiring a large linear range for the OFDM transmitter's output amplifier. In addition, OFDM is sensitive to carrier frequency offset, resulting in Inter-Carrier Interference (ICI) [50].

As a summary of this section, we outline the milestones and the main contributions found in the OFDM literature in Tables 1.1 and 1.2.

1.1.1 MIMO-Assisted OFDM

1.1.1.1 The Benefits of MIMOs

High-data-rate wireless communications have attracted significant interest and constitute a substantial research challenge in the context of the emerging WLANs and other indoor multimedia networks. Specifically, the employment of multiple antennas at both the transmitter and the receiver, which

Table 1.1: Milestones in the history of OFDM.

Year	Milestone
1957	The concept of parallel data transmission by Doelz *et al.* [17]
1966	First OFDM scheme proposed by Chang [18] for dispersive fading channels
1967	Saltzberg [19] studied a multi-carrier system employing Orthogonal QAM (O-QAM) of the carriers
1970	US patent on OFDM issued [21]
1971	Weinstein and Ebert [22] applied DFT to OFDM modems
1980	Hirosaki designed a subchannel-based equalizer for an orthogonally multiplexed QAM system [26]
	Keasler *et al.* [25] described an OFDM modem for telephone networks
1985	Cimini [29] investigated the feasibility of OFDM in mobile communications
1987	Alard and Lasalle [31] employed OFDM for digital broadcasting
1991	ANSI ADSL standard [6]
1994	ANSI HDSL standard [7]
1995	ETSI DAB standard [10]: the first OFDM-based standard for digital broadcasting systems
1996	ETSI WLAN standard [13]
1997	ETSI DVB-T standard [11]
1998	ANSI VDSL and ETSI VDSL standards [8, 9]
	ETSI BRAN standard [14]
1999	IEEE 802.11a WLAN standard [51]
2002	IEEE 802.11g WLAN standard [52]
2003	Commercial deployment of FLASH-OFDM [53, 54] commenced
2004	ETSI DVB-H standard [12]
	IEEE 802.16-2004 WMAN standard [55]
	IEEE 802.11n draft standard for next generation WLAN [56]
2005	Mobile cellular standard 3GPP Long-Term Evolution (LTE) [57] downlink
2007	Multi-user MIMO-OFDM for next-generation wireless [58]
	Adaptive HSDPA-style OFDM and MC-CDMA transceivers [59]

is widely referred to as the Multiple-Input, Multiple-Output (MIMO) technique, constitutes a cost-effective approach to high-throughput wireless communications.

The concepts of MIMOs have been under development for many years for both wired and wireless systems. One of the earliest MIMO applications for wireless communications dates back to 1984, when Winters [92] published a breakthrough contribution, where he introduced a technique of transmitting data from multiple users over the same frequency/time channel using multiple antennas at both the transmitter and receiver ends. Based on this work, a patent was filed and approved [93]. Sparked off by Winters' pioneering work [92], Salz [94] investigated joint transmitter/receiver optimization using the MMSE criterion. Since then, Winters and others [95–103] have made further significant advances in the field of MIMOs. In 1996, Raleigh [104] and Foschini [105] proposed new approaches for improving the efficiency of MIMO systems, which inspired numerous further contributions [106–114].

As a key building block of next-generation wireless communication systems, MIMOs are capable of supporting significantly higher data rates than the Universal Mobile Telecommunications System (UMTS) and the High-Speed Downlink Packet Access (HSDPA) based 3G networks [115]. As indicated by the terminology, a MIMO system employs multiple transmitter and receiver antennas for delivering parallel data streams, as illustrated in Figure 1.1. Since the information is transmitted through

Table 1.2: Main contributions on OFDM.

Year	Author(s)	Contribution
1966	Chang [18]	Proposed the first OFDM scheme
1967	Saltzberg [19]	Studied a multi-carrier system employing O-QAM
1968	Chang and Gibby [20]	Presented a theoretical analysis of the performance of an orthogonal multiplexing data transmission scheme
1970	Chang [21]	US patent on OFDM issued
1971	Weinstein and Ebert [22]	Applied DFT to OFDM modems
1980	Hirosaki [26]	Designed a subchannel-based equalizer for an orthogonally multiplexed QAM system
	Peled and Ruiz [23]	Described a reduced-complexity FD data transmission method together with a cyclic prefix technique
	Keasler *et al.* [25]	Invented an OFDM modem for telephone networks
1981	Hirosaki [27]	Suggested a DFT-based implementation of OFDM systems
1985	Cimini [29]	Investigated the feasibility of OFDM in mobile communications
1986	Hirosaki *et al.* [28]	Developed a groupband data modem using an orthogonally multiplexed QAM technique
1987	Alard and Lasalle [31]	Employed OFDM for digital broadcasting
1989	Kalet [30]	Analysed multi-tone QAM modems in linear channels
1990	Bingham [1]	Discussed various aspects of early OFDM techniques in depth
1991	Cioffi [6]	Introduced the ANSI ADSL standard
1993–1995	Warner [60], Moose [50] and Pollet [61]	Conducted studies on time and frequency synchronization in OFDM systems
1994–1996	Jones [62], Shepherd [63] and Wulich [64, 65]	Explored various coding and post-processing techniques designed for minimizing the peak power of the OFDM signal
1997	Li and Cimini [66, 67]	Revealed how clipping and filtering affect OFDM systems
	Hara and Prasad [68]	Compared various methods of combining CDMA and OFDM
1998	Li *et al.* [69]	Designed a robust Minimum Mean Square Error (MMSE) based channel estimator for OFDM systems
	May *et al.* [48]	Carried out a performance analysis of Viterbi decoding in the context of 64-Differential Amplitude and Phase-Shift Keying (64-DAPSK) and 64QAM OFDM signals
1999	Li and Sollenberger [70]	Focused on parameter estimation invoked by an MMSE diversity combiner designed for adaptive antenna array-aided OFDM
	Armour *et al.* [71–73]	Illustrated the combined OFDM equalization-aided receiver and the design of pre-Fast Fourier Transform (FFT) equalizers
	Prasetyo and Aghvami [74, 75]	Simplified the transmission frame structure for achieving fast burst synchronization in OFDM systems
	Wong *et al.* [76]	Advocated a subcarrier, bit and power allocation algorithm to minimize the total transmit power of multi-user OFDM
2000	Fazel and Fettweis [32]	A collection of state-of-the-art works on OFDM
	Van Nee and Prasad [4]	OFDM for wireless multimedia communications
	Lin *et al.* [49]	Invoked turbo coding in an OFDM system using diversity
2001–2002	Lu and Wang [77–80]	Considered channel-coded STC-assisted OFDM systems
2003	Hanzo *et al.* [3]	OFDM for broadband multi-user communications, WLANs and broadcasting
2004	Simeone *et al.* [81]	Demonstrated a subspace tracking algorithm used for channel estimation in OFDM systems
	Zhang *et al.* [82]	Adopted an Inter-Carrier Interference (ICI) cancellation scheme to combat the ICI in OFDM systems
	Necker and Stüber [83]	Exploited a blind channel estimation scheme based on the ML principle in OFDM systems
	Doufexi *et al.* [84]	Reflected the benefits of using sectorized antennas in WLANs
	Alsusa *et al.* [85]	Proposed packet-based multi-user OFDM systems using adaptive subcarrier–user allocation
2005	Williams *et al.* [86]	Evaluated a pre-FFT synchronization method for OFDM
2007	Jiang and Hanzo [58]	Multi-user MIMO-OFDM for next-generation wireless
	Hanzo and Choi [59]	Adaptive HSDPA-style OFDM and MC-CDMA transceivers
2009	Fischer and Siegl [87]	Peak-to-average power ratio reduction in single- and multi-antenna OFDM
	Mileounis *et al.* [88]	Blind identification of Hammerstein channels using QAM, PSK and OFDM inputs
	Huang and Hwang [89]	Improvement of active interference cancellation: avoidance technique for OFDM cognitive radio
	Chen *et al.* [90]	Spectrum sensing for OFDM systems employing pilot tones
	Talbot and Farhang-Boroujeny [91]	Time-varying carrier offsets in mobile OFDM

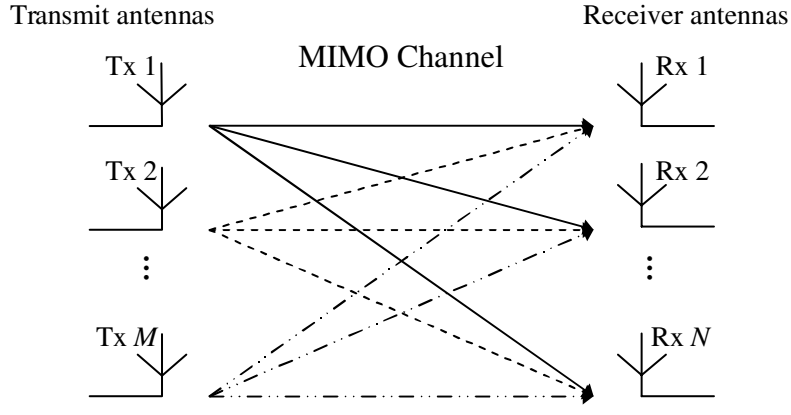

Figure 1.1: Schematic of the generic MIMO system employing M transmitter antennas and N receiver antennas. ©IEEE Jiang & Hanzo 2007 [58]

different paths, a MIMO system is capable of exploiting both transmitter and receiver diversity, hence maintaining reliable communications. Furthermore, with the advent of multiple antennas, it becomes possible to process/combine jointly the multi-antenna signals and thus improve the system's integrity and/or throughput. Briefly, compared with Single-Input, Single-Output (SISO) systems, the two most significant advantages of MIMO systems are:

1. A significant increase of both the system's capacity and spectral efficiency. The capacity of a wireless link increases linearly with the minimum of the number of transmitter or receiver antennas [104, 106]. The data rate can be increased by spatial multiplexing without consuming more frequency resources and without increasing the total transmit power.
2. Dramatic reduction of the effects of fading due to the increased diversity. This is particularly beneficial when the different channels fade independently.

An overview of MIMO techniques covering channel models, performance limits, coding and transceiver designs can be found in [116].

1.1.1.2 MIMO-OFDM

The quality of a wireless link can be described by three basic parameters, namely the transmission rate, the transmission range and the transmission reliability. Conventionally, the transmission rate may be increased by reducing the transmission range and reliability. By contrast, the transmission range may be extended at the cost of a lower transmission rate and reliability, while the transmission reliability may be improved by reducing the transmission rate and range [117]. However, with the advent of MIMO-assisted OFDM systems, the above-mentioned three parameters may be simultaneously improved [117]. Initial field tests of broadband wireless MIMO-OFDM communication systems have shown that an increased capacity, coverage and reliability is achievable with the aid of MIMO techniques [118]. Furthermore, although MIMOs can potentially be combined with any modulation or multiple-access technique, recent research suggests that the implementation of MIMO-aided OFDM is more efficient, as a benefit of the straightforward matrix algebra invoked for processing the MIMO-OFDM signals [117].

MIMO-OFDM, claimed to be invented by Airgo Networks [119], has formed the foundation of all candidate standards proposed for IEEE 802.11n [120]. In recent years, this topic has attracted substantial research efforts, addressing numerous aspects, such as system capacity [121,122], space/time/frequency coding [123–127], Peak-to-Average Power Ratio (PAPR) control [128–130], channel estimation [131–133], receiver design [134–137], etc. Recently, Paulraj *et al.* [116] and Stüber *et al.* [138] have provided

Table 1.3: Main contributions on MIMO-OFDM (Part 1).

Year	Author(s)	Contribution
2001	Piechocki *et al.* [140]	Reported on the performance benefits of spatial multiplexing using ML decoding for a Vertical Bell Labs Layered Space–Time (V-BLAST) OFDM system
	Blum *et al.* [123]	Studied improved space–time coding techniques for MIMO-OFDM systems
2002	Li [131]	Exploited optimum training sequence design and simplified channel estimation for improving the performance and reducing the complexity of channel parameter estimation in MIMO-OFDM systems
	Bolckei *et al.* [121]	Analysed the influence of physical parameters such as the amount of delay spread, cluster angle spread and total angle spread, as well as system parameters such as the number of antennas and the antenna spacing on both the ergodic capacity and outage capacity
	Catreux *et al.* [141]	Offered an overview of the challenges and promises of link adaptation in future broadband wireless networks
	Piechocki *et al.* [142]	Presented a performance evaluation of spatial multiplexing and space-frequency-coded modulation schemes designed for WLANs
	Molisch *et al.* [143]	Proposed a reduced-complexity method for grouping multiple antennas and space–time codes
	Li *et al.* [134]	Invoked space–time coding and Successive Interference Cancellation (SIC) in MIMO-OFDM systems
	Stamoulis *et al.* [144]	Revealed the effects of the ICI on MIMO-OFDM
	Doufexi *et al.* [145]	Characterized the outdoor physical layer performance of a coded MIMO-OFDM system using space–time processing
	Giangaspero *et al.* [135]	Compared two Co-Channel Interference (CCI) cancellation schemes in the context of MIMO-OFDM
2003	Li *et al.* [136]	Advocated a CCI cancellation method using angle diversity based on null-steering or minimum variance distortion response beamforming
	Bölcskei *et al.* [146]	Measured the impact of the propagation environment on the performance of space-frequency-coded MIMO-OFDM
	Barhumi *et al.* [132]	Described a Least-Squares (LS) channel estimation scheme designed for MIMO-OFDM systems based on pilot tones
	Ganesan and Sayeed [122]	Derived a virtual MIMO framework for single-transmitter, single-receiver multi-path fading channels that enables maximal exploitation of channel diversity at both the transmitter and the receiver
	Gamal *et al.* [124]	Utilized an OFDM technique to transform the MIMO multi-path channel into a MIMO flat block fading channel, where the associated diversity is exploited by employing space-frequency codes
	Moon *et al.* [128]	Evaluated the PAPR performance in a MIMO-OFDM-based WLAN system using a Space–Time Block Code (STBC)
	Cai *et al.* [147]	Developed a technique based on the autocorrelation function for estimating the Doppler spread in Rayleigh fading channels for mobile OFDM systems using multiple antennas
	Leus and Moonen [148]	Employed tone-by-tone-based equalization techniques in MIMO-OFDM systems
	Lee *et al.* [129]	Investigated the PAPR characteristics in a MIMO-OFDM system using the selective mapping approach
	Piechocki *et al.* [149]	Devised a blind method for joint detection of space–time-coded MIMO-OFDM.

compelling overviews of MIMO-OFDM communications. Furthermore, Nortel Networks developed a MIMO-OFDM prototype [139] during late 2004, which demonstrates the superiority of MIMO-OFDM over today's networks in terms of the achievable data rate. For the reader's convenience, we have summarized the major contributions on MIMO-OFDM in Tables 1.3, 1.4 and 1.5.

1.1.1.3 SDMA-based MIMO-OFDM Systems

As a subclass of MIMO arrangements, recently the Space-Division Multiple Access (SDMA) [3, 193–195] based techniques have attracted substantial interest. As one of the most promising techniques aimed at solving the capacity problem of wireless communication systems, SDMA enables multiple users to share simultaneously the same bandwidth in different geographical locations. More specifically, the exploitation of the spatial dimension, namely the so-called spatial signature, makes it possible

Table 1.4: Main contributions on MIMO-OFDM (Part 2).

Year	Author(s)	Contribution
2004	Shin *et al.* [133]	Suggested a cyclic comb-type training structure for reducing the Mean Square Errors (MSEs) at the edge subcarriers of MIMO-OFDM signals
	Xia *et al.* [150]	Created an adaptive MIMO-OFDM transmitter by applying an adaptive two-dimensional coder–beamformer with the aid of partial channel knowledge
	Huang and Letaief [151]	Portrayed an OFDM symbol-based space diversity technique
	Butler and Collings [152]	Employed an approximate log-likelihood decoding approach based on a Zero-Forcing (ZF) receiver for bit-interleaved coded-modulation-assisted MIMO-OFDM systems
	Stüber *et al.* [138]	Summarized various physical layer research challenges in MIMO-OFDM system design
	Paulraj *et al.* [116]	Provided an overview of MIMO and/or MIMO-OFDM systems
	Lu *et al.* [153]	Identified the performance of an optimized MIMO-OFDM scheme using Low-Density Parity Check (LDPC) codes
	Van Zelst and Schenk [154]	Implemented MIMO-OFDM processing and evaluated its performance by both simulations and experimental test results
	Pascual-Iserte *et al.* [155]	Conducted studies on maximizing the Signal to Noise and Interference Ratio (SNIR) over the subcarriers subject to a total transmit power constraint.
	Zeng and Ng [156]	Contrived a subspace-based semi-blind method for estimating the channel responses of a multi-user and multi-antenna OFDM uplink system
	Alien *et al.* [157]	Assessed the performance of spatial diversity in an OFDM WLAN for various antenna topologies
	Dayal *et al.* [125]	Introduced space–time channel-sounding training codes designed for multiple-antenna, non-coherent, multiple-block Rayleigh fading channel
	Park and Kang [137]	Adopted a reduced-complexity iterative algorithm for joint Maximum-A-Posteriori (MAP) detection and CCI suppression in MIMO-OFDM systems
	Tan and Stüber [158]	Combined cyclic delay diversity and MIMO-OFDM for achieving full spatial diversity in flat-fading channels
	Wang *et al.* [159]	Illustrated the diversity and coding advantages in terms of the minimum Hamming distance and the minimum squared product distance of the code as well as the relative frequencies
	Pan *et al.* [160]	Discussed dynamic spatial subchannel allocation in conjunction with adaptive beamforming in broadband OFDM wireless systems
	Tepedelenlioğlu and Challagulla [161]	Demonstrated how to achieve high diversity gains in MIMO-OFDM systems with the aid of fractional sampling
	Baek *et al.* [162]	Addressed a time-domain semi-blind channel estimation approach and a PAPR reduction scheme for MIMO-OFDM
	Dubuc *et al.* [139]	Outlined Nortel Networks' MIMO-OFDM concept prototype and provided measured performance results
	Barriac and Madhow [163]	Offered guidelines for optimizing the antenna spacing in MIMO-OFDM systems using feedback of the covariance matrix of the downlink channel

to identify the individual users, even when they are in the same time/frequency/code domains, thus increasing the system's capacity.

In Figure 1.2 we illustrate the concept of SDMA systems. As shown in Figure 1.2, each user exploiting a single-transmitter-antenna-aided Mobile Station (MS) simultaneously communicates with the BS equipped with an array of receiver antennas. Explicitly, SDMA can be considered as a specific branch of the family of MIMO systems, where the transmissions of the multiple-transmitter antennas cannot be coordinated, simply because they belong to different users. Briefly speaking, the major advantages of SDMA techniques are [196]:

- *Range extension*: With the aid of an antenna array, the coverage area of high-integrity reception can be significantly larger than that of any single-antenna-aided systems. In an SDMA system, the number of cells required to cover a given geographic area can be substantially reduced. For example, a 10-element array offers a gain of 10, which typically doubles the radius of the cell and hence quadruples the coverage area.
- *Multi-path mitigation*: Benefitting from the MIMO architecture, in SDMA systems the detrimental effects of multi-path propagations are effectively mitigated. Furthermore, in specific

Table 1.5: Main contributions on MIMO-OFDM (Part 3).

Year	Author(s)	Contribution
2005	Su *et al.* [126, 127]	Designed a general space-frequency block code structure capable of providing full-rate, full-diversity MIMO-OFDM transmission
	Zhang *et al.* [164]	Researched an optimal QR decomposition technique designed for a precoded MIMO-OFDM system using successive cancellation detection
	Yao and Giannakis [165]	Proposed a low-complexity blind Carrier Frequency Offset (CFO) estimator for OFDM systems
	Zheng *et al.* [166]	Extended Time-Division Synchronous CDMA (TD-SCDMA) to Time-Division Code-Division Multiplexing OFDM (TD-CDM-OFDM) for future 4G systems
	Yang [167]	Reviewed the state-of-the-art approaches in MIMO-OFDM air interface
	Zhang and Letaief [168]	Aimed at developing an adaptive resource allocation approach which jointly allocates subcarriers, power and bits for multi-user MIMO-OFDM systems
	Ma [169]	Established a pilot-assisted modulation scheme for CFO and channel estimation in OFDM transmissions over frequency-selective MIMO fading channels
	Fozunbal *et al.* [170]	Calculated a sphere packing lower bound and a pairwise error upper bound of the error probability of space–time frequency-coded OFDM systems using multiple antennas for transmission over block-fading channels
	Nanda *et al.* [171]	Built a MIMO WLAN prototype that provides data rates over 200 Mbps
	Kim *et al.* [172]	Invoked a QR-Decomposition combined with the M-algorithm (QRD-M) for joint data detection and channel estimation in MIMO-OFDM
	Qiao *et al.* [173]	Contrived an iterative LS channel estimation algorithm for MIMO-OFDM.
	Sampath *et al.* [174]	Validated the properties of the transmit correlation matrix through field trial results obtained from a MIMO-OFDM wireless system operated in a macro-cellular environment
	Rey *et al.* [175]	Used a Bayesian approach to design transmit prefiltering matrices for closed-loop schemes, which is robust to channel estimation errors
	Sun *et al.* [176]	Targeted the design of CFO estimator-aided Expectation Maximization (EM) based iterative receivers for MIMO-OFDM systems
	Han and Lee [130]	Provided an overview of PAPR reduction techniques for multi-carrier transmission
	Lodhi *et al.* [177]	Evaluated the complexity and performance of a Multi-Carrier Code-Division Multiple-Access (MC-CDMA) system exploiting STBCs and Cyclic Delay Diversity (CDD)
	Wang *et al.* [178]	Advanced MIMO-OFDM channel estimation using a scheme based on estimating the Time of Arrival (TOA)
	Wen *et al.* [179]	Reported on a low-complexity multi-user angle-frequency coding scheme based on the Fourier basis structure for downlink wireless systems
	Su *et al.* [180]	Performance analysis of MIMO-OFDM systems invoking coding in spatial, temporal and frequency domains
	Tan *et al.* [181]	Advocated a scheme of cross-antenna rotation and inversion utilizing additional degrees of freedom by employing multiple antennas in OFDM systems
	Park and Cho [182]	Characterized a MIMO-OFDM technique based on the weighting factor optimization for reducing the ICI caused by time-varying channels
	Shao and Roy [183]	Maximized the diversity gain achieved over frequency-selective channels by employing a full-rate space-frequency block code for MIMO-OFDM systems
	Schenk *et al.* [184]	Quantified how the transmitter/receiver phase noise affects the performance of a MIMO-OFDM system
	Borgmann and Bölcskei [185]	Contributed to the code designs for non-coherent frequency-selective MIMO-OFDM fading links
	Tarighat and Sayed [186]	Examined the effect of IQ imbalances on MIMO-OFDM systems and developed a digital signal processing framework for combating these distortions
	Jiang *et al.* [187]	Formulated a joint transceiver design combining the Geometric Mean Decomposition (GMD) with ZF-type decoders
	Choi and Heath [188]	Constructed a limited feedback architecture that combines beamforming vector quantization and smart vector interpolation
	Baek *et al.* [189]	Incorporated multiple antennas into high-rate DAB systems
2007	Jiang and Hanzo [58]	Reduced-complexity near-ML SDMA-MUDs and joint iterative channel estimation
	Hanzo and Choi [59]	Near instantaneously adaptive HSPA-style OFDM and MC-CDMA transceivers
2009	Fischer and Siegl [87]	PAPR reduction in single- and multi-antenna OFDM
	Fakhereddin *et al.* [190]	Reduced feedback and random beamforming for MIMI-OFDM
	De *et al.* [191]	Linear prediction-based semi-blind channel estimation for multi-user OFDM
	Haring *et al.* [192]	Fine frequency synchronization in the uplink of multi-user OFDM systems

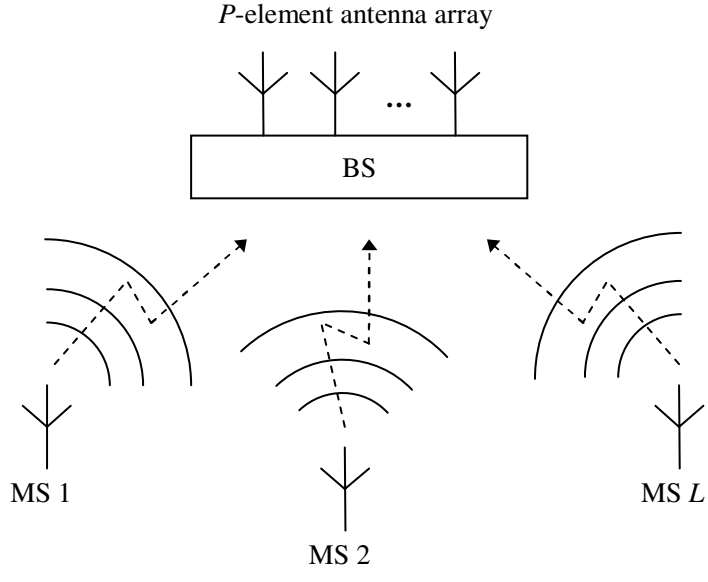

Figure 1.2: Illustration of the generic SDMA system employing a P-element receiver antenna array for supporting L mobile users. ©IEEE Jiang & Hanzo 2007 [58]

scenarios the multi-path phenomenon can even be exploited to enhance the desired users' signals by employing efficient receiver diversity schemes.

- *Capacity increase*: Theoretically, SDMA can be incorporated into any existing multiple-access standard at the cost of a limited increase in system complexity, while attaining a substantial increase in capacity. For instance, by applying SDMA to a conventional TDMA system, two or more users can share the same time slots, resulting in a doubled or higher overall system capacity.
- *Interference suppression*: The interference imposed by other systems and by users in other cells can be significantly reduced by exploiting the desired user's unique, user-specific Channel Impulse Responses (CIRs).
- *Compatibility*: SDMA is compatible with most of the existing modulation schemes, carrier frequencies and other specifications. Furthermore, it can be readily implemented using various array geometries and antenna types.

The combination of SDMA and OFDM results in SDMA-OFDM systems [3, 193, 197, 198], which exploit the merits of both SDMA and OFDM, having attracted more and more interest [198–203]. Tables 1.6 and 1.7 summarize the main contributions on SDMA and SDMA-OFDM found in the open literature.

1.2 OFDM Schematic

In this section we briefly introduce OFDM as a means of dealing with the problems of frequency-selective fading encountered when transmitting over a high-rate wideband radio channel.

In the OFDM scheme of Figure 1.3 the serial data stream of a traffic channel is passed through a serial-to-parallel converter, which splits the data into a number of parallel subchannels. The data in each subchannel are applied to a modulator, such that for M channels there are M modulators whose carrier frequencies are $f_0, f_1, \ldots, f_M$. The difference between adjacent channels is Δf and the overall bandwidth W of the N modulated carriers is $M\Delta f$.

Table 1.6: Main contributions on SDMA (Part 1).

Year	Author(s)	Contribution
1982	Yeh and Reudink [204]	Illustrated that high spectrum efficiencies can be achieved in mobile radio systems using a modest number of space diversity branches
1983	Ko and Davis [205]	Early studies on SDMA in the context of satellite communication networks
1989	Swales *et al.* [206, 207]	Devised a multi-beam adaptive BS antenna in an attempt to mitigate the problem of limited radio resources
1990	Agee *et al.* [208]	Invoked narrowband antenna arrays for blind adaptive signal extraction
1991	Anderson *et al.* [209]	Adopted adaptive antenna techniques to increase the channel capacity
1992	Balaban and Salz [210, 211]	Provided a comprehensive characterization of space diversity reception combined with various equalization techniques
1994	Xu *et al.* [212]	Offered preliminary results of experimental studies on SDMA systems
	Talwar *et al.* [213]	Described an approach for separating and estimating multiple co-channel signals with the aid of an antenna array
1995	Van Der Veen *et al.* [214]	Blindly identified Finite Impulse Response (FIR) channels using oversampling and the finite alphabet property of digital signals
	Khalaj *et al.* [215]	Estimated the spatio-temporal characteristics of the radio channel in coherent direct-sequence spread-spectrum systems
	Anand *et al.* [216]	Established a method of blind separation of co-channel Binary Phase-Shift Keying (BPSK) signals arriving at an antenna array
1997	Liu and Xu [217]	Addressed the SDMA uplink blind channel and sequence estimation problem
	Tsoulos *et al.* [218]	Reported the research of the TSUNAMI project that demonstrated the benefits of SDMA in wireless communications
1998	Deneire and Slock [219]	Derived a subspace fitting and linear prediction method using cyclic statistics of fractionally sampled channels for channel identification in multi-user and multi-antenna systems
	Tsoulos *et al.* [220, 221]	Provided an experimental demonstration of both transmit and receive beamforming supporting SDMA user access
	Barroso *et al.* [222]	Introduced a blind algorithm referred to as Array Channel-Division Multiple Access (AChDMA) for advanced SDMA in mobile communications systems
	Demmerle and Wiesbeck [223]	Designed a biconical multi-beam antenna structure for SDMA communications
	Lindmark [224]	Built a dual-polarized antenna array for an SDMA system working in the 1850–1990 MHz band
	Suard *et al.* [225]	Investigated the channel capacity enhancement of an SDMA system
	Jeng *et al.* [226]	Presented extensive experimental results of spatial signature variation using a smart antenna test bed
	Petrus *et al.* [227]	Proved that capacity improvement can be achieved using adaptive arrays at the BS of an Advanced Mobile Phone Service (AMPS) system
	Xavier *et al.* [228]	Targeted at designing a closed-form estimator for the SDMA-MIMO channel based on second-order statistics
	Farsakh and Nossek [229]	Developed an approach for jointly calculating array weights in such a way that all users receive their signals at a given SINR level
1999	Tsoulos [230]	Provided an overview of smart antennas in the context of current and future personal communication systems
	Piolini and Rolando [231]	Analysed a channel assignment algorithm for SDMA mobile systems
	Vandenameele *et al.* [193, 197, 198]	Advocated a combined SDMA-OFDM approach that couples the capabilities of the two techniques
	Galvan-Tejada and Gardiner [232, 233]	Calculated the theoretical blocking probability resulting from SDMA technology in two different channel allocation schemes
	Tsoulos [234]	Focused on TDMA air-interface techniques combined with SDMA schemes
	Vornefeld *et al.* [235]	Applied SDMA techniques to WATM systems

These M modulated carriers are then combined to give an OFDM signal. We may view the serial-to-parallel converter as applying every Mth symbol to a modulator. This has the effect of interleaving the symbols into each modulator, hence symbols $S_0, S_M, S_{2M}, \ldots$ are applied to the modulator whose carrier frequency is f_1. At the receiver the received OFDM signal is demultiplexed into M frequency bands, and the M modulated signals are demodulated. The baseband signals are then recombined using a parallel-to-serial converter.

Table 1.7: Main contributions on SDMA (Part 2).

Year	Author(s)	Contribution
2000	Djahani and Kahn [236]	Discussed the employment of multi-beam transmitters and imaging receivers in SDMA implementations
2001	Shad *et al.* [237]	Invoked dynamic slot allocation in packet-switched SDMA systems
	Kuehner *et al.* [238]	Considered a BS that communicates with smart-antenna-aided mobiles operating in multi-beam, packet-switched and SDMA modes
2002	Jeon *et al.* [239]	Contrived a smart-antenna-assisted system using adaptive beamforming for broadband wireless communications
	Bellofiore *et al.* [240, 241]	Emphasized the interaction and integration of several critical components of a mobile communication network using smart-antenna techniques
	Fang [242]	Carried out a realistic performance analysis of resource allocation schemes for SDMA systems and obtained analytical results for blocking probability.
	Arredondo *et al.* [243]	Employed a novel synthesis and prediction filter at the smart-antenna-aided BS for predicting vector channels in time-division duplex systems
	Walke and Oechtering [244]	Conducted investigations on the Cumulative Distribution Function (CDF) of the uplink carrier-to-interference ratio in a cellular radio network
	Zwick *et al.* [245]	Proposed a stochastic channel model for indoor propagations in future communication systems equipped with multiple antennas
	Zekavat *et al.* [246]	Combined smart-antenna arrays and MC-CDMA systems
	Pan and Djurić [247]	Suggested sectorized multi-beam cellular mobile communications combined with dynamic channel assignment to beams
	Cavalcante *et al.* [248]	Exploited a blind adaptive optimization criterion for SDMA detection
	Yin and Liu [249]	Developed a Medium Access Control (MAC) protocol for multimedia SDMA/TDMA packet networks
	Thoen *et al.* [199]	Showed that the performance of OFDM/SDMA processors can be significantly enhanced by adapting the constellation size applied on the individual subcarriers to the channel conditions
	Rim [250]	Examined the performance of a high-throughput downlink MIMO-SDMA technique
2003	Thoen *et al.* [200]	Utilized a Constrained Least-Squares (CLS) receiver in multi-user SDMA systems
	Alastalo and Kahola [201]	Reported link-level results of an adaptive-antenna-array-assisted system compatible with IEEE 802.11a WLANs
	Bradaric *et al.* [251]	Characterized a blind nonlinear method for identifying MIMO FIR CDMA and SDMA systems
	Alias *et al.* [202]	Constructed a Minimum Bit Error Rate (MBER) Multi-User Detector (MUD) for SDMA-OFDM systems
	Hanzo *et al.* [3]	Elaborated on channel estimation and multi-user detection techniques designed for SDMA-OFDM systems
2004	Spencer *et al.* [252]	Delivered two constrained solutions referred to as the block diagonalization and the successive optimization schemes contrived for downlink SDMA systems
	Li *et al.* [253]	Explored a low-complexity ML-based detection scheme using a so-called 'sensitive-bits' algorithm
	Choi and Murch [254]	Formulated a pre-Bell Labs Layered Space–Time (BLAST) decision feedback equalization technique for downlink MIMO channels
2005	Ajib and Haccoun [255]	Overviewed the scheduling algorithms proposed for 4G multi-user wireless networks based on MIMO technology
	Dai [203]	Performed an analysis of CFO estimation in SDMA-OFDM systems
	Nasr *et al.* [256]	Researched the estimation of the local average signal level in an indoor environment based on a 'wall-imperfection' model

The main advantage of the above OFDM concept is that because the symbol period has been increased, the channel delay spread is a significantly shorter fraction of a symbol period than in the serial system, potentially rendering the system less sensitive to ISI than the conventional serial system. In other words, in the low-rate subchannels the signal is no longer subject to frequency-selective fading, hence no channel equalization is necessary.

A disadvantage of the OFDM approach shown in Figure 1.3 is the increased complexity over the conventional system caused by employing M modulators and filters at the transmitter and M demodulators and filters at the receiver. It can be shown that this complexity can be reduced by the use of the Discrete Fourier Transform (DFT), typically implemented as a Fast Fourier Transform (FFT) [3].

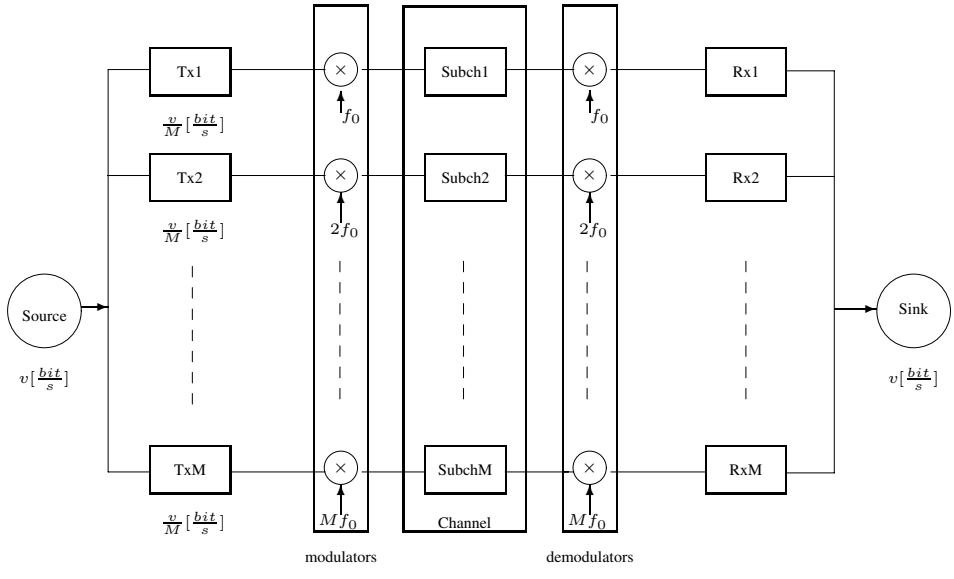

Figure 1.3: Simplified block diagram of the orthogonal parallel modem.

The subchannel modems can use almost any modulation scheme, and 4- or 16-level QAM is an attractive choice in many situations.

A schematic of the FFT-based QAM/FDM modem schematic is portrayed in Figure 1.4. The bits provided by the source are serial/parallel converted in order to form the n-level Gray-coded symbols, M of which are collected in TX buffer 1, while the contents of TX buffer 2 are being transformed by the IFFT in order to form the time-domain modulated signal. The digital-to-analogue (D/A) converted, low-pass filtered modulated signal is then transmitted via the channel and its received samples are collected in RX buffer 1, while the contents of RX buffer 2 are being transformed to derive the demodulated signal. The twin buffers are alternately filled with data to allow for the finite FFT demodulation time. Before the data is Gray coded and passed to the data sink, they can be equalized by a low-complexity method, if there is some dispersion within the narrow subbands. For a deeper tutorial exposure the interested reader is referred to [3].

1.3 Channel Estimation for Multi-carrier Systems

The ever-increasing demand for high data rates in wireless networks requires the efficient utilization of the limited bandwidth available, while supporting a high grade of mobility in diverse propagation environments. OFDM and MC-CDMA techniques [265] are capable of satisfying these requirements. This is a benefit of their ability to cope with highly time-variant wireless channel characteristics. However, as pointed out in [266], the capacity and the achievable integrity of communication systems are highly dependent on the system's knowledge concerning the channel conditions encountered. Thus, the provision of an accurate and robust channel estimation strategy is a crucial factor in achieving a high performance.

Well-documented approaches to the problem of channel estimation are constituted by *pilot-assisted*, *decision-directed* and *blind* channel estimation methods [265, 267], which are briefly summarized in Table 1.8.

Table 1.8: Major contributions addressing channel estimation in multi-carrier systems.

Year	Author(s)	Contribution
1997	Höher *et al.* [257, 258]	Cascaded 1D-FIR Wiener-filter-based channel interpolation
1998	Edfors *et al.* [259]	Detailed analysis of SVD-aided CIR-related domain noise reduction for DDCE
2000	Li [260]	DDCE using DFT-based 2D interpolation and robust prediction
	Li [261]	2D pilot pattern-aided channel estimation using 2D robust frequency-domain Wiener filtering
2001	Yang *et al.* [262]	Detailed discussion of parametric, ESPRIT-assisted channel estimation
2003	Münster and Hanzo [263]	RLS-adaptive PIC-assisted DDCE for OFDM
2004	Otnes and Tüchler [264]	Iterative channel estimation for turbo-equalization

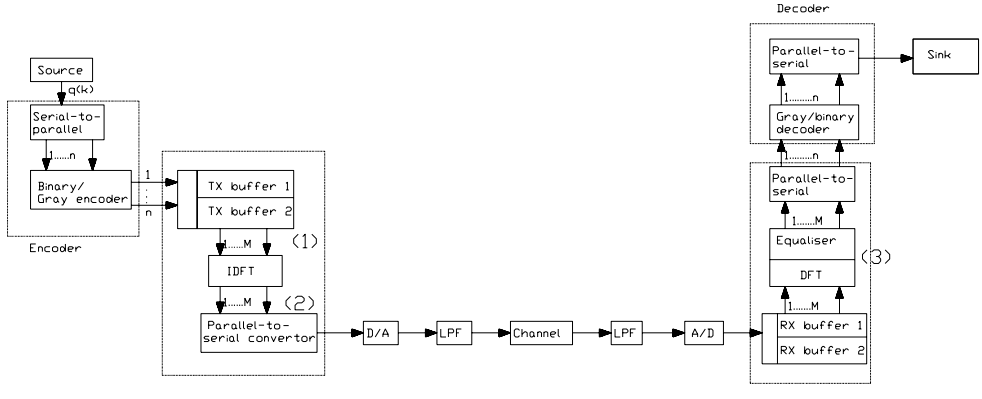

Figure 1.4: FFT-based OFDM modem schematic © Hanzo *et al.* (2003) [3].

The family of *pilot-assisted* channel estimation methods was investigated for example by Li [261], Morelli and Mengali [268], Yang *et al.* [262] as well as Chang and Su [269], where the channel parameters are typically estimated by exploiting the channel-sounding signal. For example, in OFDM and MC-CDMA often a set of frequency-domain pilots are transmitted for estimating the Frequency-Domain Channel Transfer Function (FD-CTF), which are known at the receiver [265]. The main drawback of this method is that the pilot symbols do not carry any useful information and thus they reduce the system's effective throughput.

By contrast, in Decision-Directed Channel Estimation (DDCE) methods both the pilot symbols and all the information symbols are utilized for channel estimation [265]. The simple philosophy of this method is that in the absence of transmission errors we can benefit from the availability of 100% pilot information by using the detected subcarrier symbols as an a posteriori reference signal. The employment of this method allows us to reduce the number of pilot symbols required. This technique is particularly efficient under benign channel conditions, where the probability of a decision error is low, but, naturally, this approach is also prone to error propagation effects. The family of DDCE techniques was investigated for example by van de Beek *et al.* [270], Mignone and Morello [271], Edfors *et al.* [259], Li *et al.* [260], Li and Sollenberg [272] as well as Münster and Hanzo [263, 267, 273, 274].

The class of iterative DDCE schemes, where the channel estimation is carried out through a series of iterations utilizing increasingly refined soft-decision-based feedback, was explored by

Sandell *et al.* [275], Valenti [276], Yeap *et al.* [277], Song *et al.* [278, 279], as well as by Otnes and Tüchler [264, 280].

The closely related class of joint receivers, where the channel parameters and the transmitted information-carrying symbols are estimated jointly, was explored for example by Seshadri [281], developed further by Knickenberg *et al.* [282], recently revisited by Cozzo and Hughes [283] as well as Cui and Tellambura [284, 285].

Finally, the class of *blind* estimation methods eliminates all redundant pilot symbols. Most of these methods rely on the employment of decision feedback and on the exploitation of the redundancy often found in the structure of the modulated signal, as exemplified by the techniques described for example by Antón-Haro *et al.* [286], Boss *et al.* [287], Endres *et al.* [288], Giannakis and Halford [289], Zhou and Giannakis [290] as well as by Necker and Stüber [291].

An additional major subject, closely related to channel estimation, namely the prediction of fast fading channels, was extensively studied by Haykin [292]. A so-called robust predictor was proposed by Li [260] and revised by Münster and Hanzo [274]. An adaptive RLS channel predictor was proposed by Schafhuber and Matz [293].

Subsequently, in this treatise we propose a DDCE scheme, which is suitable for employment in both OFDM and MC-CDMA systems. We analyse the achievable performance of the estimation scheme considered in conjunction with a realistic dispersive Rayleigh fading channel model having a Fractionally Spaced (FS) rather than Symbol-Spaced (SS) Power Delay Profile (PDP).

A basic component of the DDCE schemes proposed in the literature is an a posteriori Least Squares (LS) temporal estimator of the OFDM-subcarrier-related Frequency-Domain Channel Transfer Function (FD-CTF) coefficients [260, 265]. The accuracy of the resultant temporal FD-CTF estimates is typically enhanced using 1D or 2D interpolation exploiting both the time- and the frequency-domain correlation between the desired FD-CTF coefficients. The LS-based temporal FD-CTF estimator was shown to be suitable for QPSK-modulated OFDM systems [260, 265], where the energy of the transmitted subcarrier-related information symbols is constant. However, as will be pointed out in Section 7.3.1 of this treatise, the LS method cannot be readily employed in MC-CDMA systems, where – in contrast to OFDM systems – the energy of the transmitted subcarrier-related information symbols fluctuates as a function of both the modulated sequence and that of the choice of the potentially non-constant-modulus modulation scheme itself. Thus we propose an Minimum Mean Square Error (MMSE) estimation-based DDCE method, which is an appropriate solution for employment in both OFDM and MC-CDMA systems.

The system model and the channel model considered are described in Section 1.7 of this treatise. The difficulty of employing the LS approach to the problem of estimating the OFDM-subcarrier-related FD-CTF coefficients is described in Section 7.3.1. The alternative MMSE FD-CTF estimator circumventing the problem outlined in Section 7.3.1 is analysed in Section 7.3.2. Our discourse evolves further by proposing an MMSE CIR estimator exploiting the frequency-domain correlation of the FD-CTF coefficients in Section 7.4.1 and a reduced-complexity version of the CTF MMSE estimator considered is proposed in Section 7.4.2. The computational complexity of both methods is compared in Section 7.4.3.

In Section 7.4 we continue our discourse with the derivation of both the sample-spaced as well as the fractionally spaced Channel Impulse Response (CIR) estimator. In Section 7.4.5 we then perform a comparison between the two methods considered and demonstrate the advantages of the latter, i.e. fractionally spaced, scheme. Subsequently, in Section 7.5 we develop a method of parametric tracking of the fractionally spaced CIR taps, which facilitates low-complexity channel estimation in realistic channel conditions characterized by a time-variant, fractionally spaced, power delay profile. More specifically, we employ the Projection Approximation Subspace Tracking (PAST) method for the sake of recursive tracking of the covariance matrix of the Channel Transfer Function (CTF) and subsequent tracking of the corresponding CIR taps. We demonstrate that the PAST-aided decision-directed channel estimation scheme proposed exhibits good performance over the entire range of practical conditions.

In Section 7.6 we discuss two major CIR tap prediction strategies. Specifically, in Section 7.6.2 the so-called *robust* implementation of the stationary MMSE CIR predictor is considered. The *robust* CIR predictor [260] assumes a constant-valued, limited-support channel scattering function [265] during the design of the CIR tap prediction filter, and hence relies on the assumption of encountering the worst possible channel conditions. On the other hand, in Section 7.6.4 we discuss the adaptive Recursive Least-Squares (RLS) method of CIR prediction [293]. As opposed to the robust CIR predictor of [260], the RLS CIR predictor does not require any explicit information concerning the channel conditions encountered. Consequently, in Section 7.6.5 we characterize and compare the achievable performance of both methods considered and draw conclusions concerning their relative merits. Specifically, we demonstrate that the RLS prediction technique outperforms its robust counterpart over the entire range of the relevant channel conditions.

In Section 7.7 we characterize the achievable performance of the resultant PAST-aided DDCE scheme. We report an estimation efficiency of $\kappa = -18\,\text{dB}$ exhibited by a system employing 10% of pilots and communicating over a dispersive Rayleigh fading channel having a Doppler frequency of $f_D = 0.003$. Furthermore, we report a BER performance, which is only 3 dB from the corresponding BER performance exhibited by a similar system assuming perfect channel knowledge.

1.4 Channel Estimation for MIMO-OFDM

In spite of immense interest from both the academic and industrial communities, a practical MIMO transceiver architecture, capable of approaching channel capacity boundaries in realistic channel conditions, remains largely an open problem. In particular, a robust and accurate channel estimation in MIMO systems constitutes a major issue, preventing us from achieving the high capacities predicted by the relevant theoretical analysis.

Some of the major contributions addressing the problem of channel estimation in MIMO systems are summarized in Table 1.9. More specifically, a combined OFDM-SDMA approach was discussed by Vandenameele *et al.* [299]. A pilot-based approach to the problem of MIMO channel estimation has been explored by Jungnickel *et al.* in [300], by Bolcskei *et al.* [301], as well as by Zhu *et al.* [302]. On the other hand, decision-directed iterative channel estimation for MIMO systems was addressed by Li *et al.* [294, 303, 304] as well as Deng *et al.* [296]. Furthermore, s parallel interference cancellation-assisted decision-directed channel estimation scheme for MIMO-OFDM systems was proposed by Münster and Hanzo [297, 305]. Joint decoding and channel estimation for MIMO channels was considered by Grant [306] and further investigated by Cozzo and Hughes [283]. Iterative channel estimation for space–time block-coded systems was addressed by Mai *et al.* [307], while joint iterative DDCE for turbo-coded MIMO-OFDM systems was investigated by Qiao [308]. Blind channel estimation in MIMO-OFDM systems with multi-user interference was explored by Yatawatta and Petropulu [298].

Other closely related issues, namely the iterative tracking of the channel-related parameters using soft decision feedback, was studied by Sandell *et al.* [275], while iterative channel estimation in the context of turbo-equalization was considered by Song *et al.* [279], Mai *et al.* [309], as well as Otnes and Tüchler [264].

Finally, an important overview publication encompassing most major aspects of broadband MIMO-OFDM wireless communications including channel estimation and signal detection, as well as time and frequency synchronization, was contributed by Stüber *et al.* [295].

Against this background, in this treatise we propose a DDCE scheme, which is suitable for employment in a wide range of multi-antenna, multi-carrier systems as well as over the entire range of practical channel conditions. In particular, we consider mobile wireless multi-path channels, which exhibit fast Rayleigh frequency-selective fading and are typically characterized by a time-variant PDP.

We consider a generic MIMO-OFDM system employing K orthogonal frequency-domain subcarriers and having m_{t} and n_{r} transmit and receive antennas, respectively. Consequently, our MIMO channel

Table 1.9: Major contributions addressing the problem of channel estimation in MIMO systems.

Year	Author(s)	Contribution
2002	Li *et al.* [294]	MIMO-OFDM for wireless communications: signal detection with enhanced channel estimation
2004	Stüber *et al.* [295]	An important overview encompassing most of the major aspects of the broadband MIMO-OFDM wireless communications, including channel estimation, signal detection as well as time and frequency synchronization
2003	Deng *et al.* [296]	Decision-directed iterative channel estimation for MIMO systems
2003	Cozzo and Hughes [283]	Joint channel estimation and data detection in space–time communications
2005	Münster and Hanzo [297]	Parallel interference cancellation-assisted decision-directed channel estimation for OFDM systems using multiple-transmit antennas
2006	Yatawatta and Petropulu [298]	Blind channel estimation in MIMO-OFDM systems with multi-user interference

estimation scheme comprises an array of K per-subcarrier MIMO-CTF estimators, followed by an $(n_{\mathrm{r}} \times m_{\mathrm{t}})$-dimensional array of parametric CIR estimators and a corresponding array of $(n_{\mathrm{r}} \times m_{\mathrm{t}} \times L)$ CIR tap predictors, where L is the number of tracked CIR taps per link for the MIMO channel.

In Section 7.8.1 we explore a family of recursive MIMO-CTF tracking methods, which in conjunction with the aforementioned PAST-aided CIR-tracking method of Section 7.5 as well as the RLS CIR tap prediction method of Section 7.6.4, facilitate an effective channel estimation scheme in the context of an MIMO-OFDM system. More specifically, in Section 7.8.1 we consider both hard- and soft-feedback-assisted least mean squares (LMS) and recursive least-squares (RLS) tracking algorithms as well as the modified RLS algorithm, which is capable of improved utilization of the soft information associated with the decision-based estimates.

Finally, in Section 7.8.1.5 we document the achievable performance of the resultant MIMO-DDCE scheme employing recursive CTF tracking followed by the parametric CIR tap tracking and CIR tap prediction. We demonstrate that the MIMO-DDCE scheme proposed exhibits good performance over the entire range of practical conditions.

Both the Bit Error Rate (BER) as well as the corresponding MSE performance of the channel estimation scheme considered are characterized in the context of a turbo-coded MIMO-OFDM system. We demonstrate that the MIMO-DDCE scheme proposed remains effective in channel conditions associated with high terminal speeds of up to 130 km/h, which corresponds to the OFDM-symbol normalized Doppler frequency of 0.006. Additionally, we report a virtually error-free performance of a rate $1/2$ turbo-coded 8×8-QPSK-OFDM system, exhibiting a total bit rate of 8 bps/Hz and having a pilot overhead of only 10%, at an SNR of 10 dB and normalized Doppler frequency of 0.003, which corresponds to the mobile terminal speed of roughly 65 km/h.[1]

1.5 Signal Detection in MIMO-OFDM Systems

The demand for both high data rates and improved transmission integrity requires efficient utilization of the limited system resources, while supporting a high grade of mobility in diverse propagation environments. Consequently, the employment of an appropriate modulation format, as well as efficient exploitation of the available bandwidth, constitute crucial factors in achieving a high performance.

[1] Additional system parameters are characterized in Table 1.11.

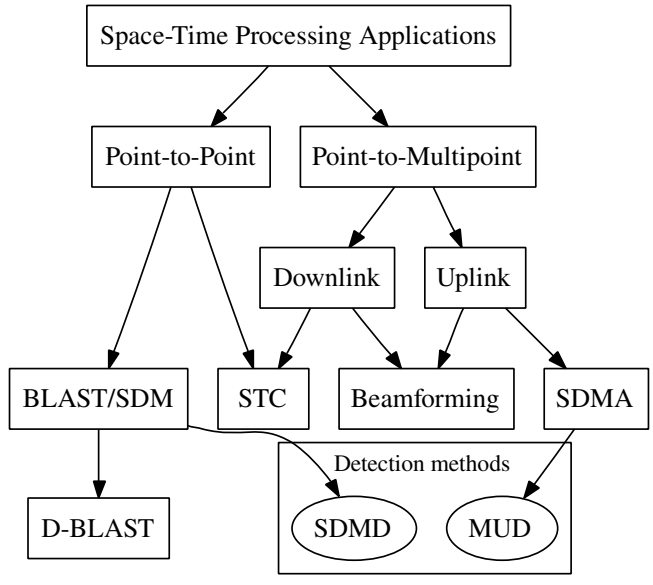

Figure 1.5: Classification of space–time processing techniques.

The OFDM modulation scheme employed in conjunction with an MIMO architecture [265], where multiple antennas are employed at both the transmitter and the receiver of the communication system, constitutes an attractive solution in terms of satisfying these requirements. Firstly, the OFDM modulation technique is capable of coping with the highly frequency-selective, time-variant channel characteristics associated with mobile wireless communication channels, while possessing a high grade of structural flexibility for exploiting the beneficial properties of MIMO architectures.

It is highly beneficial that OFDM and MIMO may be conveniently combined, since the information theoretical analysis predicts [310] that substantial capacity gains are achievable in communication systems employing MIMO architectures. Specifically, if the fading processes corresponding to different transmit–receive antenna pairs may be assumed to be independently Rayleigh distributed,[2] the attainable capacity was shown to increase linearly with the smaller of the numbers of the transmit and receive antennas [310]. Additionally, the employment of MIMO architectures allows for efficient exploitation of the spatial diversity available in wireless MIMO environments, thus improving the system's BER, as well as further increasing the system's capacity.

The family of space–time signal processing methods, which allow for the efficient implementation of communication systems employing MIMO architectures, is commonly referred to as *smart antennas*. In recent years, the concept of smart antennas has attracted intensive research interest in both the academic and industrial communities. As a result, a multiplicity of smart-antenna-related methods has been proposed. These include methods implemented at the transmitter, the receiver or both.

The classification of smart-antenna techniques is illustrated in Figure 1.5. It should be noted, however, that the classification presented here is somewhat informal and its sole purpose is to position appropriately the content of this treatise in the context of the extensive material available on the subject.

Two distinctive system scenarios employing smart antennas can be identified. The first is the so-called Space-Division Multiplexing (SDM) scenario [311], where two *peer* terminals each employ

[2]This assumption is typically regarded as valid if the appropriate antenna spacing is larger than of $\lambda/2$, where λ is the corresponding wavelength.

multiple antennas and communicate with each other over a MIMO channel, and the multiple antennas are primarily used for achieving a multiplexing gain, i.e. a higher throughput [312]. The second scenario corresponds to the Space-Division Multiple Access (SDMA) configuration [265], where a single *base station*, employing multiple antennas, communicates simultaneously using a single carrier frequency with multiple *user* terminals, each employing one or several antennas.

The various *point-to-multipoint* smart-antenna applications can be further subdivided into *uplink*- and *downlink*-related applications. The *uplink*-related methods constitute a set of techniques which can be employed in the *base station* in order to detect the signals simultaneously transmitted by multiple *user* terminals. More specifically, provided that the CIR of all users is accurately estimated, it may be used as their unique, user-specific spatial signature for differentiating them, despite communicating within the same frequency band [265]. Hence, the corresponding space–time signal processing problem is commonly referred to as Multi-User Detection (MUD) [265], while the multi-antenna, multi-user systems employing *uplink* space–time MUDs are commonly referred to as SDMA systems [265]. In contrast to the SDM-type systems designed to achieve the highest possible multiplexing gain, the design objective of the SDMA techniques is maximization of the number of users supported. By contrast, the class of beamformers [313] creates angularly selective beams for both the uplink and downlink in the direction of the desired user, while forming nulls towards the interfering users. Finally, the family of Space–Time Codes (STCs) [314] was optimized for achieving the highest possible transmit diversity gain, rather than for multiplexing gain or for increasing the number of users supported. At the time of writing, new research is aiming at achieving both the maximum attainable diversity and multiplexing gain with the aid of eigenvalue decomposition [315].

As stated above, two benefits of employing smart antennas are the system's improved integrity and the increased aggregate throughput. Hence an adequate performance criterion of the particular smart-antenna implementation is a combination of the system's attainable aggregate data throughput and the corresponding data integrity, which can be quantified in terms of the average BER. Consequently, in the context of point-to-multipoint-related smart-antenna applications, the achievable capacity associated with the particular space–time processing method considered may be assessed as a product of the simultaneously supported number of individual users and the attainable data rate associated with each supported user. The measure of data integrity may be the average BER of all the users supported. Thus, the typical objective of the multi-user-related smart-antenna implementations, such as that of an SDMA scheme, is that of increasing the number of simultaneously supported users, while sustaining the highest possible integrity of all the data communicated.

In this treatise, however, we would like to focus our attention on the family of space–time processing methods associated with the *point-to-point* system scenario. The main objective of point-to-point space–time processing is to increase the overall throughput of the system considered, as opposed to increasing the number of individual users simultaneously supported by the system, which was the case in the multi-user SDMA scenario described above. As illustrated in Figure 1.5, the family of time–space processing methods associated with the point-to-point-related smart-antenna applications entail two different approaches, namely that of STCs [314] as well as various layered space–time architectures, best known from the BLAST scheme [312].

The STC methods may be classified in two major categories, namely the Space–Time Block Code (STBC) and the Space–Time Trellis Code (STTC) categories. A simple method of STBC was first presented by Alamouti in [316]. Various STBC techniques were then extensively studied in a series of major publications by Tarokh *et al.* in [317–323] as well as by Ariyavistakul *et al.* in [324, 325]. On the other hand, the original variant of BLAST, known as the Diagonal BLAST (D-BLAST) scheme, was first introduced by Foschini in [312]. A more generic version of the BLAST architecture, the so-called Vertical BLAST (V-BLAST) arrangement, was proposed by Golden *et al.* in [326]. Furthermore, the comparative study of the D-BLAST, as well as the V-BLAST systems employing various detection techniques such as LS- and MMSE-aided Parallel Interference Cancellation (PIC), and LS- and MMSE-aided Successive Interference Cancellation (SIC), was carried out by Sweatman

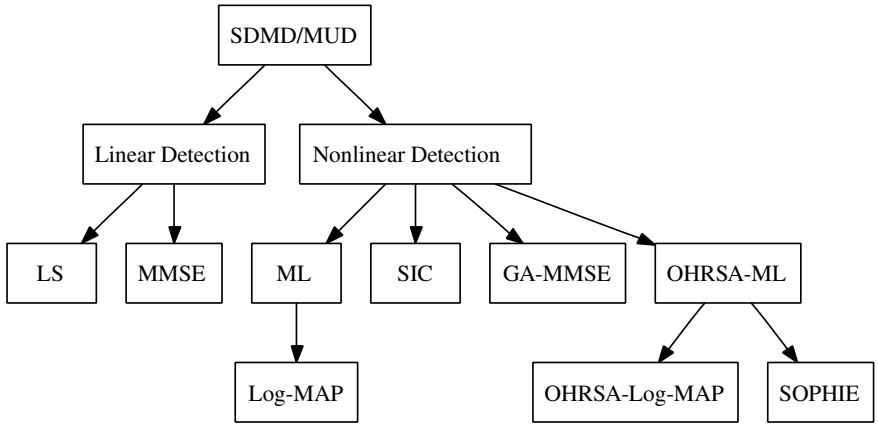

Figure 1.6: Classification of SDM detection methods.

et al. in [327]. Typically, however, the term BLAST refers to the point-to-point single-carrier MIMO architecture employing the SIC detection method, as originally proposed in [312].

For the sake of accuracy, in this work we employ the alternative terminology of SDM in order to refer to a generic MIMO architecture. The corresponding detection methods are referred to as SDM Detection (SDMD) techniques, as opposed to the MUD techniques employed in the context of SDMA systems [265]. Naturally, however, the SDMD and MUD schemes share the same signal detection methods, regardless of whether the signal arrived from multiple antennas of the same or different users. The classification of the most popular SDMD/MUD schemes is depicted in Figure 1.6. The methods considered include the linear LS and MMSE techniques, as well as nonlinear techniques, such as ML, SIC and Genetic-Algorithm-aided MMSE (GA-MMSE) [328, 329], and the novel Optimized Hierarchy Reduced Search Algorithm (OHRSA) methods proposed in this treatise.

In the course of this treatise both the MIMO channel model and the SDM-OFDM system model are described in Section 1.8. The various SDM detection methods considered are outlined in Chapter 15. Specifically, in Section 15.2.1 we demonstrate that the linear increase in capacity, predicted by information theoretical analysis [266], may indeed be achieved by employing a relatively low-complexity linear SDM detection method, such as the MMSE SDM detection technique [330]. Secondly, in Section 15.3.1 we show that a substantially better performance can be achieved by employing a nonlinear ML SDM detector [311, 331, 332], which constitutes the optimal detection method from the point of view of probabilistic sequence estimation. To elaborate a little further, the ML SDM detector is capable of attaining transmit diversity in *fully loaded* systems, where the number of transmit and receive antennas is equal. Moreover, as opposed to the linear detection schemes considered, the ML SDM detector is capable of operating in the *rank-deficient* system configuration, when the number of transmit antennas exceeds that of the receive antennas. Unfortunately, however, the excessive computational complexity associated with the exhaustive search employed by the ML detection method renders it inapplicable to practical implementation in systems having a large number of transmit antennas. Subsequently, in Sections 15.3.2 and 15.3.3 we explore a range of advanced nonlinear SDM detection methods, namely the SIC and GA-aided MMSE detection, respectively, where the latter may potentially constitute an attractive compromise between the low complexity of the linear SDM detection and the high performance of the ML SDM detection schemes. Indeed, we will demonstrate in Section 15.3.3 that the SDM detection method based on the SIC as well as on the GA-MMSE detector [329] are both capable of satisfying these requirements.

Table 1.10: Major contributions addressing sphere-decoder-aided Space–Time processing.

Year	Author(s)	Contribution
1985	Fincke *et al.* [333]	Sphere decoder technique introduced
2000	Damen *et al.* [334]	Sphere decoder was first proposed for employment in the context of space–time processing, where it was utilized for computing the ML estimates of the modulated symbols transmitted simultaneously from multiple transmit antennas.
2003	Hochwald and Brink [335]	The *complex* version of the sphere decoder
2003	Damen *et al.* [336]	Further results on the sphere decoder
2004	Pham *et al.* [337]	Improved version of the complex sphere decoder
2005	Tellambura *et al.* [338]	Multi-stage sphere decoding introduced

In Section 15.4 our discourse evolves further by proposing an enhancement of the SDMD schemes considered by employing both Space-Frequency Interleaving (SFI) and Space-Frequency Walsh–Hadamard Transform (SFWHT) spreading. The performance benefits of employing SFI and SFWHT are quantified in Section 15.4. Finally, our conclusions are summarized in Section 15.6.

PIC-assisted decision-directed channel estimation was also designed or OFDM systems using multiple transmit antennas by Münster and Hanzo [297].

Recently, a family of potent Reduced Search Algorithm (RSA) aided Space–Time processing methods has been explored (see Table 1.10). These new methods utilize the Sphere Decoder (SD) technique introduced by Fincke *et al.* [333]. The SD was first proposed for employment in the context of space–time processing by Damen *et al.* in [334], where it was utilized for computing the ML estimates of the modulated symbols transmitted simultaneously from multiple transmit antennas. The *complex* version of the SD was proposed by Hochwald and Brink in [335]. The subject was further investigated by Damen *et al.* in [336]. Subsequently, an improved version of the Complex Sphere Decoder (CSD) was advocated by Pham *et al.* in [337]. Furthermore, CSD-aided detection was considered by Cui and Tellambura in a joint channel estimation and data detection scheme explored in [284], while a revised version of the CSD method, namely the so-called Multistage Sphere Decoding (MSD), was introduced in [338]. The generalized version of the SD, which is suitable for employment in rank-deficient MIMO systems supporting more transmitters than the number of receive antennas, was introduced by Damen *et al.* in [339] and further refined by Cui and Tellambura in [340]. The so-called *fast* generalized sphere decoding was introduced by Yang *et al.* [341]. Yet another variant of SD algorithms with improved radius search was introduced by Zhao and Giannakis [342]. The subject of approaching MIMO channel capacity using soft detection on hard sphere decoding was explored by Wang and Giannakis [343]. Iterative detection and decoding in MIMO systems using sphere decoding was considered by Vikalo *et al.* [344].

Consequently, a set of novel OHRSA-aided SDM detection methods is outlined in Section 16.1. Specifically, in Section 16.1.1 we derive the OHRSA-aided ML SDM detector, which benefits from the optimal performance of the ML SDM detector [265], while exhibiting a relatively low computational complexity which is only slightly higher than that required by the low-complexity MMSE SDM detector [265]. To elaborate a little further, in Section 16.1.2 we derive a bit-wise OHRSA-aided ML SDM detector, which allows us to apply the OHRSA method of Section 16.1 in high-throughput systems which employ multi-level modulation schemes, such as M-QAM [265].

In Section 16.1.3 our discourse evolves further by deducing the OHRSA-aided Max-Log-MAP SDM detector, which allows for efficient evaluation of the soft-bit information and therefore results in highly efficient turbo decoding. Unfortunately however, in comparison with the OHRSA-aided ML SDM detector of Section 16.1.2, the OHRSA-aided Max-Log-MAP SDM detector of Section 16.1.3

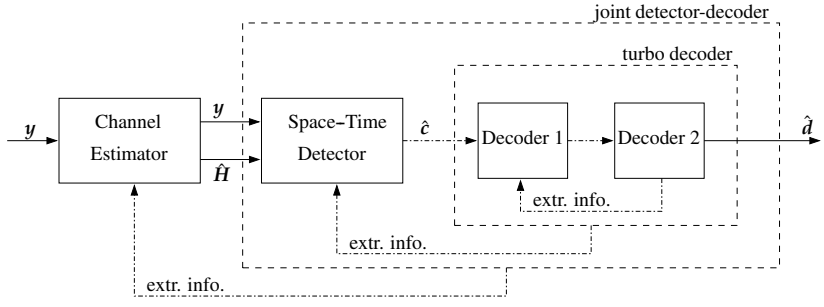

Figure 1.7: Schematic of a joint iterative receiver comprising channel estimator, SDM detector, as well as turbo decoder employing two RCS (Recursive Systematic Convolutional) serially concatenated component codes.

exhibits a substantially higher complexity. Consequently, in Section 16.1.5 we derive an approximate Max-Log-MAP method, which we refer to as Soft-output OPtimized HIErarchy (SOPHIE). The SOPHIE SDM detector combines the advantages of both the OHRSA-aided ML and OHRSA-aided Max-Log-MAP SDM detectors of Sections 16.1.2 and 16.1.3, respectively. Specifically, it exhibits a similar performance to that of the optimal Max-Log-MAP detector, while imposing a modest complexity which is only slightly higher than that required by the low-complexity MMSE SDM detector [265]. The computational complexity as well as the achievable performance of the SOPHIE SDM detector of Section 16.1.5 are analysed and quantified in Sections 16.1.5.1 and 16.1.5.2, respectively.

We will report the achievement of a BER of 10^{-4} at SNRs of $\gamma = 4.2, 9.2$ and 14.5 in high-throughput 8×8 rate $\frac{1}{2}$ turbo-coded $M = 4, 16$ and 64-QAM systems communicating over dispersive Rayleigh fading channels. Additionally, we report the achievement of a BER of 10^{-4} at SNRs of $\gamma = 9.5$, 16.3 and 22.8 in high-throughput rank-deficient 4×4, 6×4 and 8×4 rate $\frac{1}{2}$ turbo-coded 16-QAM systems, respectively.

1.6 Iterative Signal Processing for SDM-OFDM

In spite of immense interest from both the academic and industrial communities, a practical MIMO transceiver architecture, capable of approaching channel capacity boundaries in realistic channel conditions, remains largely an open problem. An important overview publication encompassing most major aspects of broadband MIMO-OFDM wireless communications including channel estimation and signal detection, as well as time and frequency synchronization, was contributed by Stüber *et al.* [295]. Other important publications considering MIMO systems in realistic conditions include those by Münster and Hanzo [297], Li *et al.* [294], Mai *et al.* [307] as well as Qiao *et al.* [308]. Nevertheless, substantial contributions addressing all the major issues inherent to MIMO transceivers, namely error correction, space–time detection and channel estimation in realistic channel conditions, remain scarce.

Against this background, in Section 17.1 we derive an iterative, so-called *turbo* Multi-Antenna, Multi-Carrier (MAMC) receiver architecture. Our turbo-receiver is illustrated in Figure 1.7. Following the philosophy of turbo processing [314], our turbo SDM-OFDM receiver comprises a succession of detection modules, which iteratively exchange soft-bit-related information and thus facilitate a substantial improvement in the overall system performance.

More specifically, our turbo SDM-OFDM receiver comprises three major components, namely the soft-feedback decision-directed channel estimator, discussed in detail in Section 7.8, followed by the soft-input, soft-output OHRSA Log-MAP SDM detector derived in Section 16.1.3 as well as a soft-input, soft-output serially concatenated turbo code [345]. Consequently, in this chapter we would like

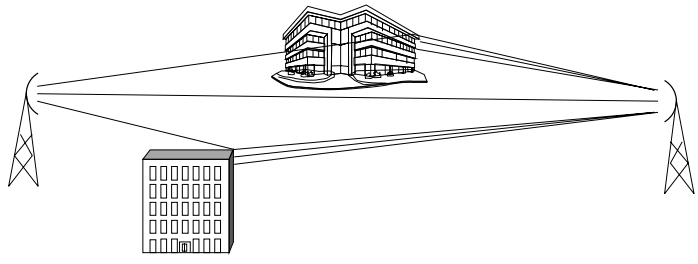

Figure 1.8: Illustration of a wireless multi-path communication link. Note that the non-line-of-sight paths randomly fade as a result of the diffraction induced by scattering surfaces.

to analyse the achievable performance of each individual constituent of our turbo receiver, as well as the achievable performance of the entire iterative system. Our aim is to identify the optimum system configuration, while considering various design trade-offs, such as achievable error-rate performance, achievable data rate and associated computational complexity.

In Section 17.4.2.4 we demonstrate that our turbo SDM-OFDM system employing the MIMO-DDCE scheme of Section 7.8 as well as the OHRSA Log-MAP SDM detector of Section 16.1.3 remains effective in channel conditions associated with high terminal speeds of up to 130 km/h, which corresponds to the OFDM symbol normalized Doppler frequency of 0.006. Additionally, we report a virtually error-free performance for a rate $1/2$ turbo-coded 8×8 QPSK-OFDM system, exhibiting an effective throughput of $8\,\text{MHz} \cdot 8\,\text{bps/Hz} = 64\,\text{Mbps}$ and having a pilot overhead of only 10% at an SNR of 7.5 dB and a normalized Doppler frequency of 0.003, which corresponds to a mobile terminal speed of about 65 km/h.

1.7 System Model

1.7.1 Channel Statistics

A SISO wireless communication link as seen in Figures 1.8 and 1.9 is constituted by a multiplicity of statistically independent components, termed *paths*. Thus, such a channel is referred to as a multi-path channel. A multi-path channel is typically characterized by its Power Delay Profile (PDP), which is a set of parameters constituted by the paths' average powers σ_l^2 and the corresponding relative delays τ_l. Some examples of commonly used PDPs are illustrated in Figure 1.10. The physical interpretation of each individual path is a single distortionless ray between the transmitter and the receiver antennas. While the term PDP corresponds to the average power values associated with the different multi-path channel components, the term CIR refers to the instantaneous state of the dispersive channel encountered and corresponds to the vector of the instantaneous amplitudes $\alpha_l[n]$ associated with different multi-path components. Thus, the statistical distribution of the CIR is determined by the channel's PDP. In the case of independently Rayleigh fading multiple paths we have $\alpha_l[n] \in \mathcal{CN}(0, \sigma_l^2),\ l = 1, 2, \ldots, L$, where $\mathcal{CN}(0, \sigma^2)$ is a complex Gaussian distribution having mean 0 and variance σ^2.

The individual scattered and delayed signal components usually arise as a result of refraction or diffraction from scattering surfaces, as illustrated in Figure 1.8, and are termed Non-Line-Of-Sight (NLOS) paths. In most recently proposed wireless mobile channel models, each such CIR component α_l associated with an individual channel path is modelled by a Wide-Sense Stationary (WSS) narrowband complex Gaussian process [348] having correlation properties characterized by the cross-correlation function

$$r_\alpha[m, j] = \mathtt{E}\{\alpha_i[n]\alpha_j^*[n-m]\} = r_{t;i}[m]\delta[i-j], \tag{1.1}$$

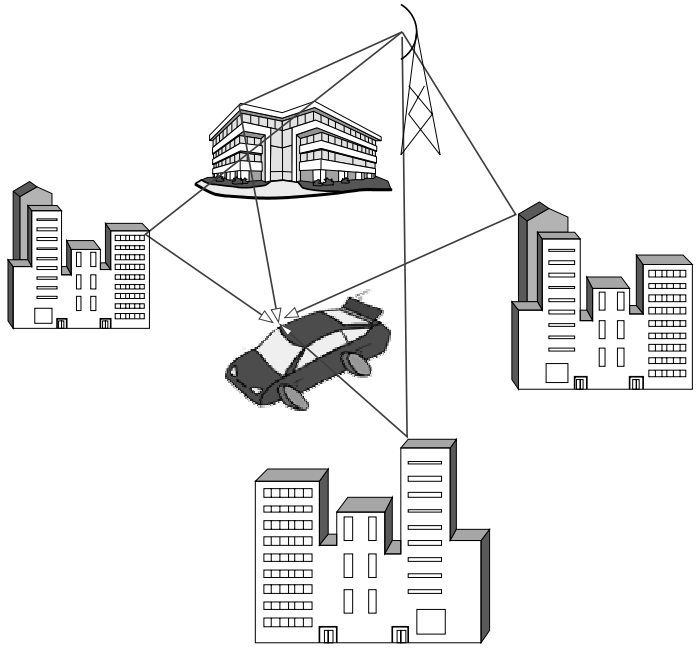

Figure 1.9: Illustration of a wireless multi-path communication link. Note that the non-line-of-sight paths randomly fade as a result of the diffraction induced by scattering surfaces.

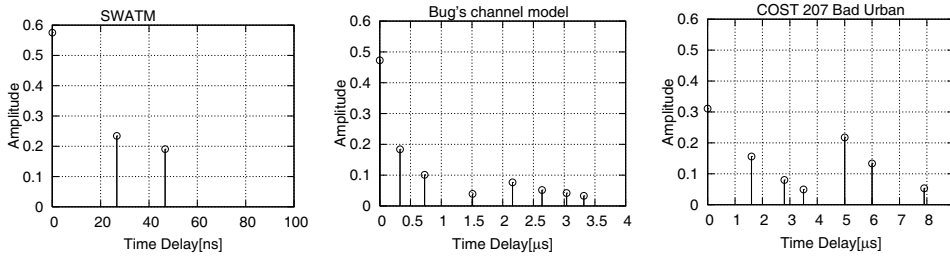

(a) (b) (c)

Figure 1.10: PDPs corresponding to three different channel models: namely (a) the Short Wireless Asynchronous Transfer Mode (SWATM) channel model of [265]; (b) Bug's channel model [346]; and (c) the COST-207 Bad Urban (BU) channel model defined for UMTS-type systems, as characterized in [347].

where n is a discrete OFDM-block-related time-domain index and $\delta[\cdot]$ is the Kronecker delta function. The above equation suggests that the different CIR components are assumed to be mutually uncorrelated and each exhibits time-domain autocorrelation properties defined by the time-domain correlation function $r_{t;i}[m]$. The Fourier transform pair of the correlation function $r_t[n]$ associated with each CIR tap corresponds to a band-limited Power Spectral Density (PSD) $p_t(f)$, such that $p_t(f) = 0$ if $|f| > f_D$, where f_D is termed the *maximum Doppler frequency*. The time period $1/f_{\rm D}$ is the so-called *coherence time* of the channel [348] and usually $1/f_{\rm D} \gg T$, where T is the duration of the OFDM block.

A particularly popular model of the time-domain correlation function $r_t[n]$ was proposed by Jakes in [349] and is described by

$$r_t[n] = r_J[n] = J_0(nw_d), \tag{1.2}$$

where $J_0(x)$ is a zero-order Bessel function of the first kind and $w_d = 2\pi T f_D$ is the normalized Doppler frequency. The corresponding U-shaped PSD function, termed the Jakes spectrum, is given by [349]

$$p_J(w) = \begin{cases} \frac{2}{w_d} \frac{1}{\sqrt{1-(w/w_d)^2}}, & \text{if } |w| < w_d \\ 0, & \text{otherwise.} \end{cases}$$

Generally speaking, the Doppler frequencies f_D can assume different values for different signal paths. However, as was advocated in [260], for the sake of exploiting the time-domain correlation in the context of channel parameter estimation and prediction, it is sufficient to make a worst-case assumption about the nature of time-domain correlation of the channel parameters encountered. The associated worst-case channel time-domain correlation properties can be characterized by an ideally band-limited Doppler PSD function given by [260, 265]

$$p_t(f) = p_{B,unif}(f) = \begin{cases} \frac{1}{2f_D}, & \text{if } |f| < f_D \\ 0, & \text{otherwise,} \end{cases} \tag{1.3}$$

where f_D is the assumed value of the maximum Doppler frequency over all channel paths. The corresponding time-domain correlation function can be described as

$$r_t[m] = r_B[m] = \frac{\sin 2\pi f_D m}{2\pi f_D m}. \tag{1.4}$$

We adopt the complex baseband representation of the continuous-time CIR, as given by [348]

$$h(t,\tau) = \sum_l \alpha_l(t) c(\tau - \tau_l), \tag{1.5}$$

where $\alpha_l(t)$ is the time-variant complex amplitude of the lth path and the τ_l is the corresponding path delay, while $c(\tau)$ is the aggregate impulse response of the transmitter–receiver pair, which usually corresponds to the raised-cosine Nyquist filter. From (1.5) the continuous CTF can be described as in [304]

$$\begin{aligned} H(t,f) &= \int_{-\infty}^{\infty} h(t,\tau) e^{-\jmath 2\pi f \tau}\, d\tau \\ &= C(f) \sum_l \alpha_l(t) e^{-\jmath 2\pi f \tau_l}, \end{aligned} \tag{1.6}$$

where $C(f)$ is the Fourier transform pair of the transceiver impulse response $c(\tau)$ characterized in Figure 1.11.

As was pointed out in [260], in OFDM/MC-CDMA systems using a sufficiently long cyclic prefix and adequate synchronization, the discrete subcarrier-related CTF can be expressed as

$$H[n,k] = H(nT, k\Delta f) = C(k\Delta f) \sum_{l=1}^{L} \alpha_l[n] W_K^{k\tau_l/T_s} \tag{1.7}$$

$$= \sum_{m=0}^{K_0-1} h[n,m] W_K^{km}, \tag{1.8}$$

where $T_s = T/K$ is the baseband sample duration, while K_0 is the length of the cyclic prefix, which normally corresponds to the maximum delay spread encountered, such that $K_0 > \tau_{max}/T_s$.

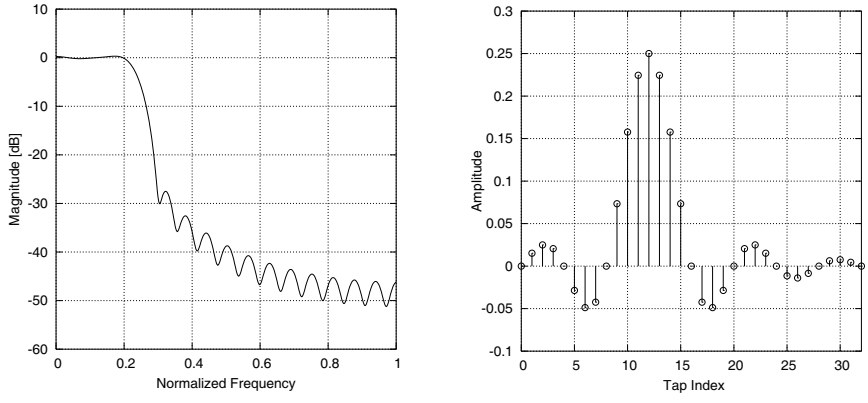

(a) (b)

Figure 1.11: (a) Frequency response and (b) impulse response of an order 8 raised-cosine shaping filter with an oversampling rate of 4, a roll-off factor of 0.2 and a delay of three samples.

Subsequently

$$h[n,m] = h(nT, mT_s) = \sum_{l=1}^{L} \alpha_l[n] c(mT_s - \tau_l) \tag{1.9}$$

is the Sample-Spaced CIR (SS-CIR) and $W_K = \exp(-\jmath 2\pi/K)$. Note that in realistic channel conditions associated with non-sample-spaced time-variant path delays $\tau_l(n)$, the receiver will encounter dispersed received signal components in several neighbouring samples owing to the convolution of the transmitted signal with the system's impulse response, which we refer to as leakage. This phenomenon is usually unavoidable and therefore the resultant SS-CIR $h[n,m]$ will be constituted by numerous correlated non-zero taps described by Equation (1.5) and illustrated in Figure 1.12. By contrast, the Fractionally Spaced CIR (FS-CIR) $\alpha_l[n] = \alpha_l(nT)$ will be constituted by a lower number of $L \ll K_0 \ll K$ non-zero, statistically independent taps associated with distinctive propagation paths, as depicted in Figure 1.12.

As shown in [260], the cross-correlation function $r_H[m,l]$, which characterized both the time- and frequency-domain correlation properties of the discrete CTF coefficients $H[n,k]$ associated with different OFDM blocks and subcarriers, can be described as

$$\begin{aligned} r_H[m,l] &= \mathtt{E}\{H[n+m,k+l]H^*[n,k]\} \\ &= \sigma_H^2 r_t[m] r_f[l], \end{aligned} \tag{1.10}$$

where $r_t[m]$ is the time-domain correlation function described by Equation (1.4), while $r_f[i]$ is the frequency-domain correlation function, which can be expressed as follows [261]:

$$r_f[l] = |C(l\Delta f)|^2 \sum_{i=1}^{L} \frac{\sigma_i^2}{\sigma_H^2} e^{-\jmath 2\pi l \Delta f \tau_i}, \tag{1.11}$$

where $\sigma_H^2 = \sum_{i=1}^{L} \sigma_i^2$.

1.7.2 Realistic Channel Properties

The majority of existing advanced channel estimation methods rely on a priori knowledge of the channel statistics commonly characterized by the channel's PDP for the sake of estimating the instantaneous CIR

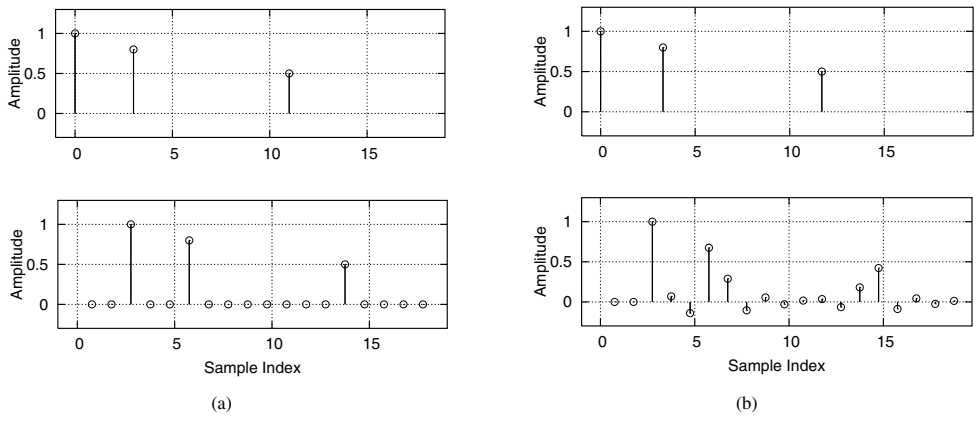

Figure 1.12: The **FS-CIR** (top) and the effective **SS-CIR** (bottom) resulting from the convolution of the original FS-CIR with the raised-cosine FIR of Figure 1.11 for the cases of (a) sample-spaced and (b) fractionally spaced power delay profiles.

and the corresponding CTF. It is evident, however, that in realistic wireless mobile channels, where at least one of the communicating terminals is in motion, the channel's PDP will also become time variant and thus may not be a priori known at the receiver.

For the sake of designing as well as characterizing the performance of an efficient and robust channel estimation scheme, which will be suitable for realistic channel conditions, we propose a channel model which sustains the important characteristics of the realistic wireless mobile channels. More specifically, as opposed to the conventional constant PDP, our channel model is characterized by a time-variant PDP, where both the relative delays τ_l and the corresponding average powers σ_l^2 of different PDP taps vary with time.

Our channel model is dynamically generated using the geometric scattering model illustrated in Figure 1.13. More specifically, the individual scatterers associated with different propagation paths are randomly generated using a Markov statistical model. The corresponding relative delays τ_l and powers σ_l^2 associated with each propagation path are calculated based on the geometrical location of each of the scatterers. Correspondingly, the rate of change in the values of the PDP tap delays τ_l is determined by the speed of the mobile wireless terminal and is characterized by the PDP *tap drift rate* parameter ν_τ. The specific assumptions regarding the practical range of values of the parameter ν_τ are discussed in the next chapter. Furthermore, each propagation path experiences independent fast Rayleigh fading. Finally, the set of parameters characterizing the Markov model employed is chosen such that the average channel statistics correspond to the desired static-PDP channel model.

1.7.3 Baseline Scenario Characteristics

As a baseline scenario we consider a mobile wireless communication system utilizing a frequency bandwidth of $B = 10\,\mathrm{MHz}$ at a carrier frequency of $f_c = 2.5\,\mathrm{GHz}$. Furthermore, we assume an OFDM system having $K = 128$ orthogonal subcarriers. The corresponding FFT frame duration is $T_s = K/B = 16\,\mu\mathrm{s}$. We assume a cyclic prefix of $1/4T_s = 4\,\mu\mathrm{s}$ and thus a total OFDM symbol duration of $T = 20\,\mu\mathrm{s}$.

Some other important system-related assumptions include the relative speed of the communicating terminals, which we assume not to exceed $v = 130\,\mathrm{km/h} = 36\,\mathrm{m/s}$. Furthermore, the OFDM-symbol-normalized Doppler frequency f_D relates to the relative speed of the communicating terminals

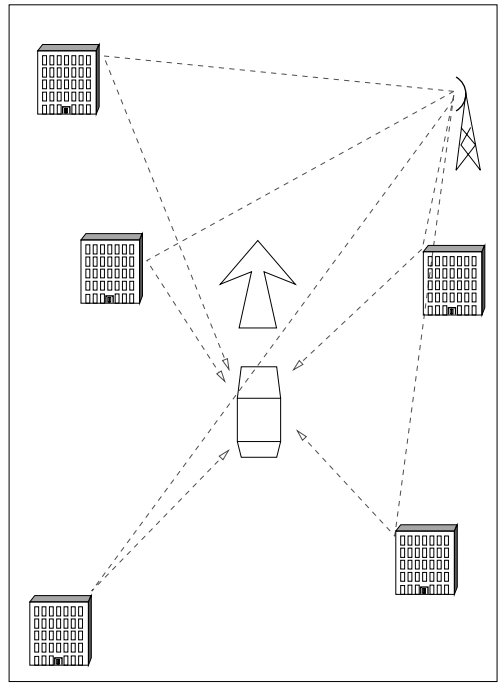

Figure 1.13: Corresponding PDP examples.

as follows:

$$f_D = T\frac{vf_c}{c}, \tag{1.12}$$

where $c = 3 \times 10^8$ m/s denotes the speed of light. The actual Doppler frequency f_D/T encountered in the mobile wireless environment is assumed to be in the range of 3 to 300 Hz, where the maximum value of 300 Hz corresponds to the relative terminal speed of $v = 130$ km/h and the carrier frequency of $f_c = 2.5$ GHz. Finally, the OFDM-symbol-normalized PDP tap drift speed ν_τ may be calculated as follows:

$$\nu_\tau = T\frac{v}{c}, \tag{1.13}$$

which suggests that the value of the PDP tap drift speed parameter does not exceed the maximum value of $\nu_\tau = 2.4 \times 10^{-6}\,\mu\text{s} = T \cdot 0.12\,\mu\text{s/s}$.

The resultant baseline scenario system characteristics are summarized in Table 1.11.

1.7.4 MC Transceiver

The transmitter part of the system typically consists of an OFDM/MC-CDMA encoder and modulator, the output of which is a complex-valued baseband time-domain signal. The resultant baseband signal is oversampled and pulse shaped using a Nyquist filter, such as, for example, the root-raised-cosine filter characterized in Figure 1.11. The resultant oversampled signal is then converted into an analogue passband signal using a D/A converter and upconverted to the RF band. At the receiver side a reciprocal process is taking place, where the received RF signal is amplified by the RF frontend and downconverted to an intermediate-frequency passband, then sampled by the A/D converter, downconverted to the

Table 1.11: Baseline scenario system characteristics.

Parameter	Value
Carrier frequency f_c	2.5 GHz
Channel bandwidth B	8 MHz
Number of carriers K	128
FFT frame duration T_s	16 μs
OFDM symbol duration T	20 μs (4 μs of cyclic prefix)
Max. delay spread τ_{max}	4 μs
Max. terminal speed v	130 km/h
Norm. Max. Doppler spread f_D	$0.006 = T \cdot 300$ Hz
Norm. Max. PDP tap drift ν_τ	2.4×10^{-6} μs $= T \cdot 0.12$ μs/s

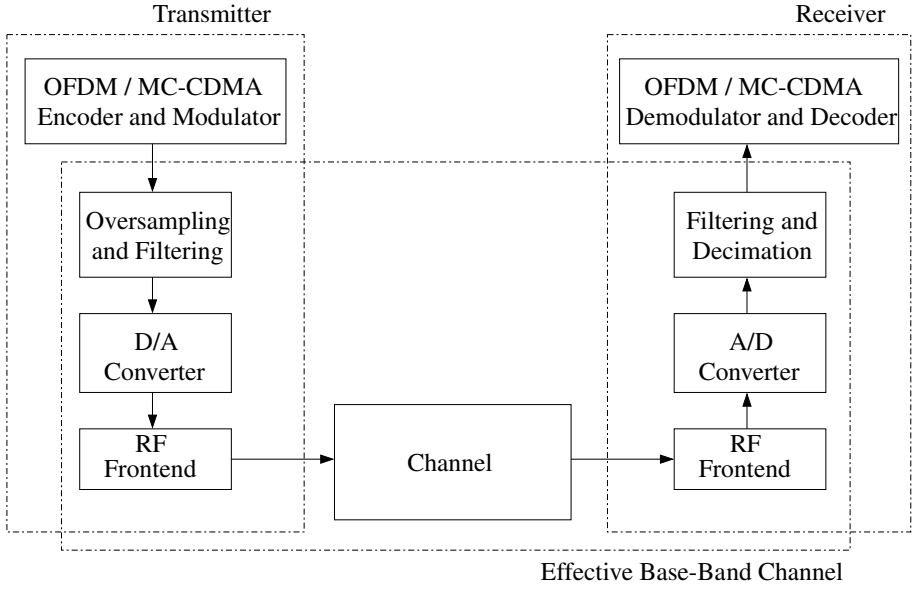

Figure 1.14: Schematic illustration of a typical OFDM/MC-CDMA system's PHY layer.

baseband, filtered by a matched Nyquist filter and finally decimated. The resultant complex-valued baseband signal is processed by the corresponding OFDM/MC-CDMA demodulator and decoder block, where the transmitted information symbols are detected.

In this treatise we consider the link between the output of the MC modulator and the input of the MC demodulator of Figure 1.14 as an *effective baseband channel*. The proof of feasibility for this assumption is beyond the scope of this contribution; however, it can be found for example in [348, 350].

The discrete frequency-domain model of the OFDM/MC-CDMA system illustrated in Figure 1.14 can be described as in [304]

$$y[n,k] = H[n,k]x[n,k] + w[n,k], \tag{1.14}$$

for $k = 0, \ldots, K-1$ and all n, where $y[n,k]$, $x[n,k]$ and $w[n,k]$ are the received symbol, the transmitted symbol and the Gaussian noise sample respectively, corresponding to the kth subcarrier of the nth OFDM block. Furthermore, $H[n,k]$ represents the complex-valued CTF coefficient associated

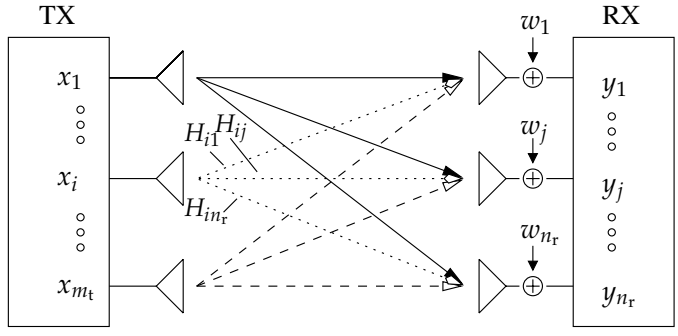

Figure 1.15: Illustration of a MIMO channel constituted by m_t transmit and n_r receive antennas. The corresponding MIMO channel is characterized by the $(n_r \times m_t)$-dimensional matrix $\mathbf{H}$ of CTF coefficients.

with the kth subcarrier and time instance n. Note that in the case of an M-QAM modulated OFDM system, $x[n,k]$ corresponds to the M-QAM symbol accommodated by the kth subcarrier, while in an MC-CDMA system, such as a Walsh–Hadamard Transform (WHT) assisted OFDM scheme using a G-chip WH spreading code and hence capable of supporting G users [265], we have

$$x[n,k] = \sum_{p=0}^{G-1} c[k,p]s[n,p], \tag{1.15}$$

where $c[k,p]$ is the kth chip of the pth spreading code, while $s[n,p]$ is the M-QAM symbol spread by the pth code. Each of the G spreading codes is constituted by G chips.

1.8 SDM-OFDM System Model

1.8.1 MIMO Channel Model

We consider a MIMO wireless communication system employing m_t transmit and n_r receive antennas; hence, the corresponding MIMO wireless communication channel is constituted by $(n_r \times m_t)$ propagation links, as illustrated in Figure 1.15. Furthermore, each of the corresponding $(n_r \times m_t)$ SISO propagation links comprises a multiplicity of statistically independent components, termed *paths*. Thus, each of these SISO propagation links can be characterized as a *multi-path* SISO channel, discussed in detail in Section 1.7.1. Similarly to the SISO case, the multi-carrier structure of our SDM-OFDM transceiver allows us to characterize the broadband frequency-selective channel considered as an OFDM subcarrier-related vector of flat-fading CTF coefficients. However, as opposed to the SISO case, for each OFDM symbol n and subcarrier k the MIMO channel is characterized by an $(n_r \times m_t)$-dimensional matrix $\mathbf{H}[n,k]$ of the CTF coefficients associated with the different propagation links, such that the element $H_{ij}[n,k]$ of the CTF matrix $\mathbf{H}[n,k]$ corresponds to the propagation link connecting the jth transmit and ith receive antennas.

Furthermore, the correlation properties of the MIMO-OFDM channel can be readily derived as a generalization of the SISO-OFDM channel scenario discussed in detail in Section 1.7.1. As shown in [260], the cross-correlation function $r_H[m,l]$, which characterizes both the time- and frequency-domain correlation properties of the discrete CTF coefficients $H_{ij}[n,k]$ associated with the particular (i,j)th propagation link of the MIMO channel, as well as with the different OFDM symbol and

subcarrier indices n and k, can be described as

$$\begin{aligned} r_{H;ij}[m,l] &= \mathrm{E}\{H_{ij}^{*}[n+m,k+l], H_{ij}[n,k]\} \\ &= \sigma_H^2 r_t[m] r_f[l], \end{aligned} \tag{1.16}$$

where $r_t[m]$ is the time-domain correlation function, which may be characterized by the time-domain correlation model proposed by Jakes in [349], where we have

$$r_t[m] = r_J[m] = J_0(nw_d), \tag{1.17}$$

and $J_0(x)$ is a zero-order Bessel function of the first kind, while $w_d = 2\pi T f_D$ is the normalized Doppler frequency. On the other hand, the frequency-domain correlation function $r_f[l]$ can be expressed as follows [261]:

$$r_f[l] = |C(l\Delta f)|^2 \sum_{i=1}^{L} \frac{\sigma_i^2}{\sigma_H^2} e^{-j2\pi l \Delta f \tau_i}, \tag{1.18}$$

where $C(f)$ is the frequency response of the pulse-shaping filter employed by the particular system, σ_i^2 and τ_i, $i = 1, \ldots, L$, are the average power and the corresponding delay of the L-tap PDP encountered, while σ_H^2 is the average power per MIMO channel link, such that $\sigma_H^2 = \sum_{i=1}^{L} \sigma_i^2$.

In this discussion we assume the different MIMO channel links to be mutually uncorrelated. This common assumption is usually valid if the spacing between the adjacent antenna elements exceeds $\lambda/2$, where λ is the wavelength corresponding to the RF signal employed. Thus, the overall cross-correlation function between the (i,j)th and (i',j')th propagation links may be described as

$$\begin{aligned} r_{H;ij;i'j'}[m,l] &= \mathrm{E}\{H_{i'j'}^{*}[n+m,k+l], H_{ij}[n,k]\} \\ &= \sigma_H^2 r_t[m] r_f[l] \delta[i-i'] \delta[j-j'], \end{aligned} \tag{1.19}$$

where $\delta[i]$ is the discrete Kronecker delta function.

1.8.2 Channel Capacity

While most of the multi-path NLOS channel models can be collectively categorized as Rayleigh fading, different channel models characterized by different PDPs exhibit substantial differences in terms of their *information-carrying capacity* and *potential diversity gain*. The channel's capacity determines the upper bound for the overall system's throughput. On the other hand, the available diversity gain allows the communication system to increase its transmission integrity. Various modulation and coding schemes can be employed by the communication system in order to increase its spectral efficiency and also to take advantage of diversity. Some of these methods are widely discussed in the literature, e.g. in [351], and include the employment of antenna arrays, space–time coding, time- and frequency-domain spreading, channel coding, time- and frequency-domain repetition, etc. The theoretical performance boundaries of such methods are discussed in [266, 352]. Furthermore, the trade-offs between the attainable system capacity gain and the corresponding diversity gain are addressed in [353].

Consequently, the unrestricted capacity of a generic single-carrier ergodic-flat-fading MIMO channel can be expressed as in [335], where

$$\mathcal{C} = \mathrm{E}\left\{ \log \det \left[\sigma_w^2 \mathbf{I} + \frac{1}{m_{\mathrm{t}}} \mathbf{H}\mathbf{H}^{\mathrm{H}} \right] \right\}, \tag{1.20}$$

where $\mathbf{H}$ is an $(n_{\mathrm{r}} \times m_{\mathrm{t}})$-dimensional matrix with independent complex Gaussian-distributed entries.

In realistic communication systems, however, the achievable throughput is limited by the modulation scheme employed. Some examples of such modulation schemes are M-ary PSK or M-ary QAM constellation schemes, where M is the number of complex symbols constituting the constellation map corresponding to the particular modulation scheme employed. The upper bound defining the maximum

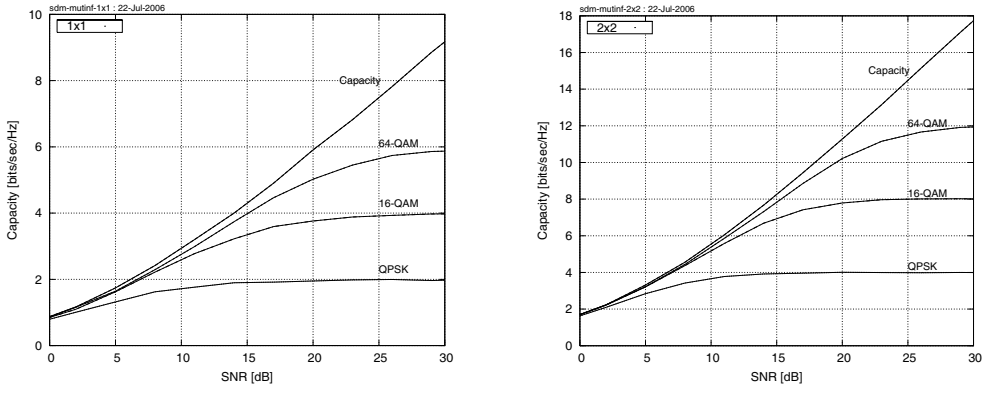

(a) (b)

Figure 1.16: Capacity $\mathcal{C}$ of Equation (1.20) as well as mutual information $I(\mathbf{s};\mathbf{y})$ of Equation (1.21) versus SNR for (a) 1×1 and (b) 2×2 systems in Rayleigh uncorrelated flat fading.

throughput achievable by a particular discrete modulation scheme was first discussed by Shannon in [354] and was shown to be determined by the mutual information $I(\mathbf{s};\mathbf{y})$ exhibited by the modulation scheme employed. The mutual information can be calculated using the following expression:

$$I(\mathbf{s};\mathbf{y}) = H(\mathbf{y}) - H(\mathbf{y}|\mathbf{s}), \tag{1.21}$$

where $H(\cdot) = -\mathrm{E}\log p(\cdot)$ denotes the entropy function [354]. In the case of having a Gaussian i.i.d. noise sample vector $\mathbf{w}$ with the corresponding covariance matrix given by $C_w = \sigma_w^2\mathbf{I}$, the constrained entropy constituent $H(\mathbf{y}|\mathbf{s})$ of Equation (1.21) is expressed as follows [335]:

$$H(\mathbf{y}|\mathbf{x}) = n_\mathrm{r}\log 2\pi\sigma_w^2 e, \tag{1.22}$$

whereas the unconstrained entropy constituent $H(\mathbf{y})$ can be approximated numerically using a Monte Carlo simulation as in [335], where

$$H(\mathbf{y}) = -\mathrm{E}\log\left(\frac{1}{M^{m_\mathrm{t}}(2\pi\sigma_w^2)^{n_\mathrm{r}}}\sum_{\mathbf{s}}\exp\left[-\frac{1}{2\sigma_w^2}\|\mathbf{y}-\mathbf{H}\mathbf{s}\|^2\right]\right), \tag{1.23}$$

where the expectation is taken over the three sources of randomness in the choice of $\mathbf{s}, \mathbf{H}$ and $\mathbf{w}$. Moreover, the summation in Equation (1.23) is carried out over all M^{m_t} possible values of $\mathbf{s}$.

Figures 1.16(a) and 1.16(b) characterize both the capacity $\mathcal{C}$ of Equation (1.20) as well as the mutual information $I(\mathbf{s};\mathbf{y})$ of Equation (1.21) for SISO and 2×2 MIMO systems, respectively. The mutual information plots depicted in both figures correspond to systems employing QPSK as well as 16- and 64-QAM modulations.

1.8.3 SDM-OFDM Transceiver Structure

The schematic of a typical SDM-OFDM system's physical layer is depicted in Figure 1.17. The transmitter of the SDM-OFDM system considered is typically constituted by the encoder and modulator seen in Figure 1.17, generating a set of m_t complex-valued baseband time-domain signals [265]. The modulated baseband signals are then processed in parallel. Specifically, they are oversampled and shaped using a Nyquist filter, such as for example a root-raised-cosine filter. The resultant oversampled signals are then converted into an analogue passband signal using a bank of D/A converters and

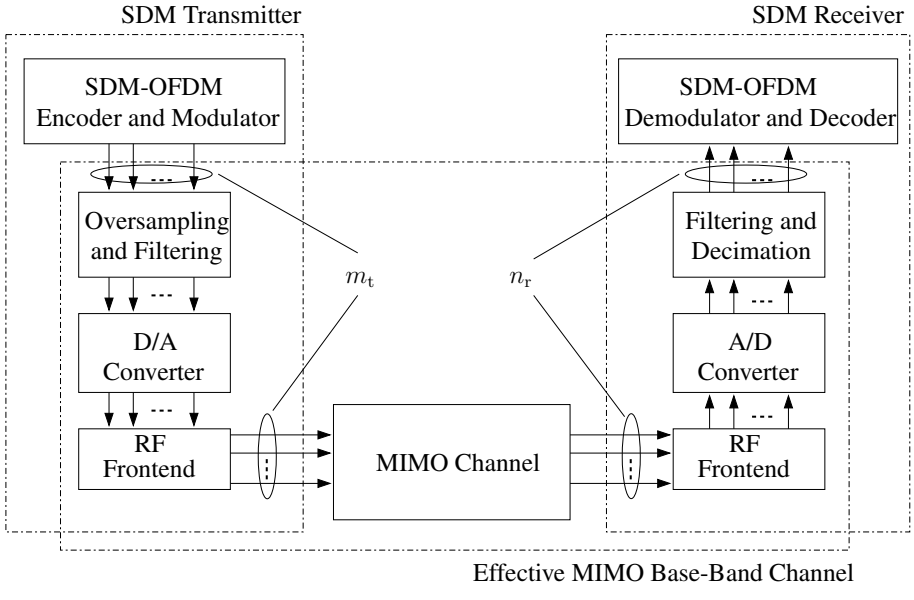

Figure 1.17: Schematic of a typical SDM-OFDM system's physical layer.

upconverted to the RF band. At the receiver side of the SDM-OFDM transceiver, the inverse process takes place, where the set of received RF signals associated with the n_r receive antenna elements is amplified by the RF amplifier and downconverted to an intermediate-frequency passband. The resultant passband signals are then sampled by a bank of A/D converters, downconverted to the baseband, filtered by a matched Nyquist filter and finally decimated, in order to produce a set of discrete complex-valued baseband signals. The resultant set of discrete signals is processed by the corresponding demodulator and decoder module seen in Figure 1.17, where the transmitted information-carrying symbols are detected.

In this treatise we consider the link between the output of the SDM-OFDM modulator and the input of the corresponding SDM-OFDM demodulator of Figure 1.17 as an effective baseband MIMO channel. The proof of feasibility for this assumption is beyond our scope here, but it can be found for example in [348, 350]. The structure of the resultant baseband SDM-OFDM system is depicted in Figure 1.18, where the bold grey arrows illustrate subcarrier-related signals represented by the vectors $\mathbf{x}_i$ and $\mathbf{y}_i$, while the thin black arrows accommodate scalar time-domain signals.

The discrete frequency-domain model of the SDM-OFDM system, illustrated in Figure 1.18, may be characterized as a generalization of the SISO case described in Section 1.7.1. That is, we have

$$y_i[n,k] = \sum_{j=1}^{m_t} H_{ij}[n,k]x_j[n,k] + w_i[n,k], \tag{1.24}$$

where $n = 0, 1, \ldots$ and $k = 0, \ldots, K-1$ are the OFDM symbol and subcarrier indices, respectively, while $y_i[n,k]$, $x_j[n,k]$ and $w_i[n,k]$ denote the symbol received at the ith receive antenna, the symbol transmitted from the jth transmit antenna and the Gaussian noise sample encountered at the ith receive antenna, respectively. Furthermore, $H_{ij}[n,k]$ represents the complex-valued CTF coefficient associated with the propagation link connecting the jth transmit and ith receive antennas at the kth OFDM subcarrier and time instance n. Note that in the case of an M-QAM modulated OFDM system, $x_j[n,k]$ corresponds to the M-QAM symbol accommodated by the kth subcarrier of the nth OFDM symbol transmitted from the jth transmit antenna element.

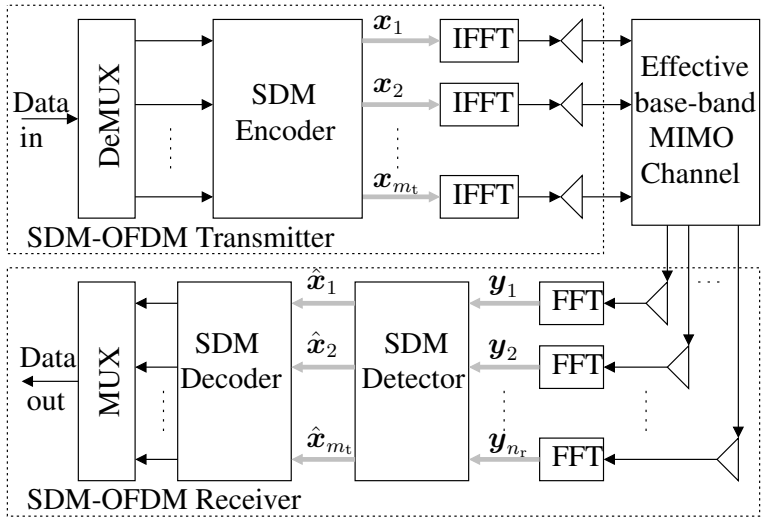

Figure 1.18: Schematic of a generic SDM-OFDM BLAST-type transceiver.

The SDM-OFDM system model described by Equation (1.24) can be interpreted as the per-OFDM-subcarrier vector expression of

$$\mathbf{y}[n,k] = \mathbf{H}[n,k]\mathbf{x}[n,k] + \mathbf{w}[n,k], \tag{1.25}$$

where we introduce the space-division-related vectors $\mathbf{y}[n,k]$, $\mathbf{x}[n,k]$ and $\mathbf{w}[n,k]$, as well as a space-division-related $(n_r \times m_t)$-dimensional matrix of CTF coefficients $\mathbf{H}[n,k]$. Note that, similarly to the SISO case, the multi-carrier structure of the SDM-OFDM transceiver allows us to represent the broadband frequency-selective MIMO channel as a subcarrier-related vector of flat-fading MIMO-CTF matrices $\mathbf{H}[n,k]$.

1.9 Novel Aspects and Outline of the Book

Having briefly reviewed the OFDM, MIMO-OFDM and SDMA-OFDM literature, let us now outline the organization of this monograph:

- **Chapter 3: Channel Coding Assisted STBC-OFDM Systems**
  As an introductory study, in this chapter we discuss various channel-coded Space–Time Block Codes (STBCs) in the context of single-user and single-carrier OFDM systems. This work constitutes the background for the multi-user systems to be investigated in the following chapters. More specifically, various Turbo Convolutional (TC) codes, Low-Density Parity Check (LDPC) codes and Coded Modulation (CM) schemes are combined with STBCs to improve the performance of the single-user system considered.

- **Chapter 4: Coded Modulation Assisted Multi-user SDMA-OFDM Using Frequency-Domain Spreading**
  In this chapter, we invoke a multi-user MIMO SDMA-OFDM system for uplink communications, where the classic Minimum Mean Square Error (MMSE) Multi-User Detector (MUD) is employed at the BS for separating the different users' signals. The CM schemes discussed in Chapter 3, namely Trellis-Coded Modulation (TCM), Turbo TCM (TTCM), Bit-Interleaved Coded Modulation (BICM) and Iteratively Decoded BICM (BICM-ID), are evaluated and

compared in the context of the SDMA-OFDM system. Furthermore, the performance gain arising from invoking Walsh–Hadamard Transform Spreading (WHTS) across a block of OFDM subcarriers in the Frequency Domain (FD) is studied in both the uncoded SDMA-OFDM and the CM-assisted SDMA-OFDM systems.

- **Chapter 5: Hybrid Multi-user Detection for SDMA-OFDM Systems**
  This chapter focuses on the design of MUDs invoked by the SDMA receiver. Specifically, the Maximum Likelihood Detection (MLD) scheme is found to attain the best performance at the cost of a computational complexity that increases exponentially both with the number of users and with the number of Bits Per Symbol (BPS) transmitted by higher-order modulation schemes. By contrast, the MMSE MUD exhibits a lower complexity at the expense of a performance loss. In order to achieve a good performance–complexity trade-off, Genetic Algorithm (GA) based MUD techniques are proposed for employment in channel-coded SDMA-OFDM systems, where TTCM is used. Moreover, a novel Biased Q-function Based Mutation (BQM) assisted Iterative GA (IGA) MUD is designed. The performance of the proposed BQM-IGA is compared with both that of the optimum MLD and the linear MMSE MUD in the so-called fully loaded and overloaded scenarios, respectively, where the number of users is equal to or higher than the number of receiver antenna elements. Additionally, the computational complexity associated with the various MUD schemes is discussed.
- **Chapter 6: Direct-Sequence Spreading and Slow Subcarrier-Hopping Aided Multi-user SDMA-OFDM Systems**
  This chapter commences with a short review of conventional SDMA-OFDM systems, followed by an introduction to hybrid SDMA-OFDM arrangements, which incorporate Direct-Sequence Spreading (DSS) and/or Frequency-Hopping (FH) techniques into conventional SDMA-OFDM. A novel FH technique referred to as Slow SubCarrier Hopping (SSCH) is designed for hybrid DSS/FH SDMA-OFDM systems using a TTCM scheme. Furthermore, two types of SSCH pattern are discussed, namely the Random SSCH (RSSCH) and the Uniform SSCH (USSCH) patterns. The performance of the proposed TTCM-assisted DSS/SSCH SDMA-OFDM system is evaluated and compared with the conventional SDMA-OFDM and various hybrid SDMA-OFDM configurations.
- **Chapter 7: Channel Estimation for OFDM and MC-CDMA**
  We derive an advanced Decision Directed Channel Estimation (DDCE) scheme, which is capable of recursive tracking and prediction of rapidly fluctuating channel parameters, characterized by time-variant statistics. More specifically, we employ a Projection Approximation Subspace Tracking (PAST) [355] technique for the sake of tracking the channel transfer function's low-rank signal subspace and thus facilitating a high-accuracy tracking of the channel's transfer function, while imposing a relatively low computational complexity.
- **Chapter 8: Iterative Joint Channel Estimation and MUD for SDMA-OFDM Systems**
  The objective of this chapter is to develop an efficient solution to the channel estimation problem of multi-user MIMO-OFDM systems. It is well known that, compared with SISOsystems, channel estimation in the MIMO scenario becomes more challenging, owing to the increased number of independent transmitter–receiver links to be estimated. Against this background, an iterative, joint channel estimation and symbol detection approach is proposed for LDPC-coded MIMO SDMA-OFDM systems. More specifically, the method modifies the GA MUD advocated in Chapter 5 so that it becomes capable of jointly optimizing the Frequency-Domain CHannel Transfer Functions (FD-CHTFs) and the multi-user data symbols. Moreover, an efficient algorithm is derived, which enables the GA to output soft bits for the sake of improving the performance of the LDPC channel decoder.
- **Chapter 9: Reduced-Complexity Sphere Detection for Uncoded SDMA-OFDM Systems**
  The main objective of this chapter is systematically to review the fundamentals of the SD, which is considered to be one of the most promising low-complexity near-optimum detection

techniques at the time of writing. Furthermore, we address the SD-related complexity reduction issues. Specifically, the principle of the Hard-Input, Hard-Output (HIHO) SD is reviewed first in the context of both the depth-first and breadth-first tree search based scenarios, along with that of the GSD, which is applicable to challenging rank-deficient MIMO scenarios. A comprehensive comparative study of the complexity reduction schemes devised for different types of SDs, namely the conventional depth-first SD, the K-best SD and the novel OHRSA detector, is carried out by analysing their conceptual similarities and differences. Finally, their achievable performance and the complexity imposed by the various types of SDs are investigated in comparison with each other.

- **Chapter 10: Reduced-Complexity Iterative Sphere Detection for Channel-Coded SDMA-OFDM Systems**
  The fundamentals of the LSD scheme are studied at the beginning of this chapter in the context of an iterative detection aided channel-coded MIMO-OFDM system. Potentially excessive complexity may be imposed by the conventional LSD, since it has to generate soft information for every transmitted bit, which requires the observation of a high number of hypotheses about the transmitted MIMO symbol. Based on the above-mentioned complexity issue, we contrive a generic centre-shifting SD scheme and the so-called a priori-LLR-threshold assisted SD scheme with the aid of EXIT chart analysis, both of which are capable of effectively reducing the potentially high complexity imposed by the SD-aided iterative receiver. Moreover, we combine the above-mentioned schemes in the interest of further reducing the complexity imposed. In addition, for the sake of enhancing the achievable iterative detention gains and hence improving the bandwidth efficiency, a Unity-Rate Code (URC) assisted three-stage, serially concatenated transceiver employing the so-called Irregular Convolutional Codes (IrCCs) is devised. Finally, the benefits of the proposed centre-shifting SD scheme are also investigated in the context of the above-mentioned three-stage iterative receiver.
- **Chapter 11: Sphere-Packing Modulated STBC-OFDM and its Sphere Detection**
  In this chapter we extend the employment of the turbo-detected Sphere Packing (SP) aided Space–Time Block Coding (STBC) scheme to Multi-User MIMO (MU-MIMO) scenarios, because SP was demonstrated to be capable of providing useful performance improvements over conventionally modulated orthogonal design-based STBC schemes in the context of Single-User MIMO (SU-MIMO) systems. For the sake of achieving a near-MAP performance, while imposing a moderate complexity, we specifically design the K-best SD scheme for supporting the operation of the SP-modulated system, since the conventional SD cannot be directly applied to such a system. Consequently, when relying on our SD, a significant performance gain can be achieved by the SP-modulated system over its conventionally modulated counterpart in the context of MU-MIMO systems.
- **Chapter 12: Multiple-Symbol Differential Sphere Detection for Cooperative OFDM**
  The principle of the MSDSD is first reviewed, as recently proposed for mitigating the time-selective channel-induced performance loss suffered by classic direct transmission schemes employing the Conventional Differential Detection (CDD) scheme. Then, we specifically design the MSDSD for both the Differential Amplify-and-Forward (DAF) and Differential Decode-and-Forward (DDF) assisted cooperative systems based on the multi-dimensional tree search proposed in Chapter 4, which is capable of achieving a significant performance gain for transmission over time-selective channels induced by the relative mobility among the cooperating transceivers.
- **Chapter 13: Resource Allocation for the Differentially Modulated Cooperative UL**
  In this chapter the theoretical BER performance of both the DAF- and DDF-aided cooperative cellular uplinks is investigated. Then, based on the minimum BER criterion, we design efficient Cooperating-User Selection (CUS) and Adaptive-Power Allocation (APA) schemes for the above-mentioned two types of differentially modulated cooperative systems, while requiring

no Channel State Information (CSI) at the receiver. Moreover, we investigate the Cooperative-Protocol Selection (CPS) of the uplink system in conjunction with a beneficial CUS as well as the APA scheme in order to improve further the achievable end-to-end performance, leading to a resource-optimized hybrid cooperative system. Hence, a number of cooperating MSs may be adaptively selected from the available MS candidate pool and the cooperative protocol employed by a specific cooperating MS may also be adaptively selected in the interest of achieving the best possible BER performance.

- **Chapter 14: The Near-Capacity Differentially Modulated Cooperative Cellular Uplink**
  The DDF-aided cooperative system's DCMC capacity is investigated in comparison with that of its classic direct-transmission-based counterpart in order to answer the grave fundamental question of whether it is worth introducing cooperative mechanisms into the development of wireless networks, such as the cellular voice and data networks. Then, we propose a practical framework for designing a cooperative system which is capable of performing close to the network's corresponding non-coherent DCMC capacity. Based on our low-complexity, near-capacity design criterion, a novel Irregular Distributed Hybrid Concatenated Differential (Ir-DHCD) coding scheme is contrived for the DDF cooperative system employing our proposed capacity-achieving, low-complexity, adaptive-window-aided, SISO iterative MSDSD scheme.
- **Chapter 15: Multi-stream Detection for SDM-OFDM Systems**
  The multi-stream detection problem of SDM-OFDM systems is similar to the MUD techniques of SDMA-OFDM arrangements, which are classified and reviewed in this chapter.
- **Chapter 16: Approximate Log-MAP SDM-OFDM Multi-stream Detection**
  We propose the novel family of Optimized Hierarchy Reduced Search Algorithm (OHRSA) aided space–time processing methods, which may be regarded as an advanced extension of the Complex Sphere Decoder (CSD) method, portrayed in [337]. The algorithm proposed extends the potential application range of the CSD methods of [335] and [337], as well as reducing the associated computational complexity. Moreover, the OHRSA-aided SDM detector proposed exhibits the near-optimum performance of the Log-MAP SDM detector, while imposing a substantially lower computational complexity, which renders it an attractive design alternative for practical systems.
- **Chapter 17: Iterative Channel Estimation and Multi-stream Detection for SDM-OFDM**
  Finally, we propose an iterative turbo-receiver architecture, which utilizes both the soft-decision feedback-aided MIMO channel estimation scheme of Chapter 7 as well as the Log-MAP SDM detection method derived in Chapter 16. Additionally, we carry out an analysis of the associated design trade-offs.
- **Chapter 18: Summary, Conclusions and Future Research**
  The major findings of our work are summarized in this chapter, including our suggestions for future research.

1.10 Chapter Summary

The historic development of various MIMO techniques was briefly summarized in Section 1.1.1.1, followed by a rudimentary introduction to MIMO-OFDM systems in Section 1.1.1.2. In Section 1.1.1.3 a concise review of various SDMA and SDMA-OFDM techniques was given, highlighting the associated signal processing problems.